



Multistability and Transient Dynamics on Networked Systems

Der Fakultät für Mathematik & Naturwissenschaften
der Carl von Ossietzky Universität Oldenburg
zur Erlangung des Grades und Titels
Doktor der Naturwissenschaften (Dr. rer. nat.)
angenommene Dissertation

von

Kalel Luiz Rossi

geboren am 13.10.1997 in Curitiba, Parana, Brasilien

Gutachter: Prof. Dr. Ulrike Feudel

Gutachter: Prof. Dr. Klaus Lehnertz

Tag der Disputation:

Contents

List of Publications	4
Abstract	6
Zusammenfassung	8
1 Methodology	9
1.1 Basics of dynamical systems theory	9
1.1.1 Dynamical systems and the uniqueness and existence of their solutions	9
1.1.2 The fate of linear dynamical systems	9
1.1.3 The fate of nonlinear dynamical systems I: attractors	10
1.1.4 Formalizing attractors and basins	12
1.1.5 Invariant manifolds: structures that organize state space	14
1.1.6 The fate of nonlinear dynamical systems II: multistability and basins of attraction	16
1.1.7 How to find attractors	18
1.2 Basics of bifurcations	19
1.2.1 Saddle-node bifurcation of equilibria	20
1.2.2 Hopf bifurcation	21
1.2.3 Homoclinic bifurcation	22
1.3 Basics of network theory	22
1.4 Basics of Kuramoto oscillators	25
1.4.1 Derivation of the model and transition to synchronization	25
1.4.2 Multistability in homogeneous case: twisted states	27
2 Small changes at single nodes can shift global network dynamics	30
2.1 Introduction	30
2.2 Methodology	33
2.3 Results	34
2.3.1 Introduction to dynamical malleability	34
2.3.2 Comprehensive view of dynamical malleability	36
2.3.3 Unpredictability of dynamical malleability	40
2.3.4 Ratio of short to long-range connections	41
2.3.5 Multistability	42
2.3.6 Distributions of samples	43
2.4 Discussions and conclusions	45
3 Conclusions	51
Acknowledgments	66
Eidesstattliche Erklärung	67

List of Publications

This dissertation is based on the following publications:

Chapter 2.1.7: George Datseris, Kalel L. Rossi, and Alexandre Wagemakers. Framework for global stability analysis of dynamical systems. *Chaos* **33**, 073151 (2023).

Statement of authorship:

George Datseris: Conceptualization (lead); Investigation (equal); Formal analysis (equal); Software (equal); Visualization (lead); Writing – original draft (equal); Writing – review & editing (equal).

Kalel Luiz Rossi: Conceptualization (equal); Formal analysis (equal); Software (equal); Visualization (equal); Writing – original draft (equal); Writing – review & editing (equal).

Alexandre Wagemakers: Conceptualization (equal); Formal analysis (equal); Software (equal); Writing – original draft (equal); Writing – review & editing (equal).

Chapter 3: Kalel L. Rossi, Roberto C. Budzinski, Bruno R. R. Boaretto, Lyle E. Muller, and Ulrike Feudel. Small changes at single nodes can shift global network dynamics. *Physical Review Research* **5**, 013220 (2023).

Statement of authorship:

Kalel Luiz Rossi: Conceptualization (equal); Investigation (lead); Formal analysis (lead); Software (lead); Visualization (lead); Writing – original draft (lead); Writing – review & editing (lead).

Roberto C. Budzinski: Conceptualization (equal); Investigation (equal); Formal analysis (equal); Writing – original draft (equal); Writing – review & editing (equal).

Bruno R. R. Boaretto: Conceptualization (equal); Investigation (equal); Formal analysis (equal); Writing – original draft (equal); Writing – review & editing (equal).

Lyle E. Muller: Conceptualization (equal); Investigation (equal); Formal analysis (equal); Writing – review & editing (equal).

Ulrike Feudel: Conceptualization (equal); Investigation (equal); Formal analysis (equal); Writing – original draft (equal); Writing – review & editing (equal); Supervision (lead).

Chapter 4: Kalel L. Rossi, Everton S. Medeiros, Peter Ashwin and Ulrike Feudel. Transients versus network interactions give rise to multistability through trapping mechanism.

Statement of authorship:

Kalel Luiz Rossi: Conceptualization (equal); Investigation (lead); Formal analysis (lead); Software (lead); Visualization (lead); Writing – original draft (lead); Writing – review & editing (lead).

Everton S. Medeiros: Conceptualization (equal); Investigation (equal); Formal analysis (equal); Writing – original draft (equal); Writing – review & editing (equal).

Peter Ashwin: Investigation (supporting); Formal analysis (equal); Writing – review & editing (equal).

Ulrike Feudel: Conceptualization (equal); Investigation (equal); Formal analysis (equal); Writing – original draft (equal); Writing – review & editing (equal); Supervision (lead).

Chapter 5: Kalel L. Rossi, Roberto C. Budzinski, Everton S. Medeiros, Bruno R. R. Boaretto, Lyle E. Muller, and Ulrike Feudel. Dynamical properties and mechanisms of metastability: a perspective in neuroscience.

Statement of authorship:

Kalel Luiz Rossi: Conceptualization (equal); Investigation (lead); Formal analysis (lead); Software (lead); Visualization (lead); Writing – original draft (lead); Writing – review & editing (lead).

Roberto C. Budzinski: Conceptualization (equal); Investigation (equal); Formal analysis (equal); Writing – original draft (equal); Writing – review & editing (equal).

Everton S. Medeiros: Conceptualization (equal); Investigation (equal); Formal analysis (equal); Writing – original draft (equal); Writing – review & editing (equal).

Bruno R. R. Boaretto: Conceptualization (equal); Investigation (equal); Formal analysis (equal); Writing – original draft (equal); Writing – review & editing (equal).

Lyle E. Muller: Conceptualization (equal); Investigation (supporting); Formal analysis (supporting); Writing – review & editing (equal).

Ulrike Feudel: Conceptualization (equal); Investigation (equal); Formal analysis (equal); Writing – original draft (equal); Writing – review & editing (equal); Supervision (lead).

On top of these main thesis papers, I have also collaborated in other works, which resulted in two further publications, with me as a co-author. They are not included in this thesis.

- Bruno R. R. Boaretto, Roberto C. Budzinski, Kalel L. Rossi, Thiago L. Prado, Sergio R. Lopes and Cristina Masoller. Temporal Correlations in Time Series Using Permutation Entropy, Ordinal Probabilities and Machine Learning. *Entropy* **23**, 1025 (2021).
- Bruno R.R. Boaretto, Roberto C. Budzinski, Kalel L. Rossi, Cristina Masoller, Elbert E.N. Macau. Spatial permutation entropy distinguishes resting brain states. *Chaos, Solitons and Fractals* **171**, 113453 (2023).

Abstract

Many systems in nature and in theory display emergent behavior, in which relatively simple subunits interact together to create a complicated global behavior that is not present in any of the units alone. An important phenomenon that can be emergent is multistability, the coexistence of many stable solutions - attractors - in a dynamical system with fixed parameters. Multistability is observed for instance in power grids, brain circuits and ecological networks. It has important consequences: a multistable system operating on a particularly desirable attractor may not be safe, as a perturbation in the state of the system can cause it to switch to another coexisting attractor. On the other hand, coexistence of attractors may be useful for systems performing computations such as memory. In networked systems, multistability can arise from the interactions of the multiple subunits, but the specific mechanisms that generate it are not fully known. Multistability can coexist with another emergent phenomenon in networked systems: synchronization, in which the interactions between units cause them to adjust their rhythms toward a collective motion. For instance, frequency synchronization occurs when units with different natural frequencies lock their oscillations onto a common frequency. It may also happen that the phases of their oscillations cluster together, in a phenomenon called phase synchronization. Synchronized attractors can coexist with each other and with unsynchronized attractors. In this case, understanding the robustness of the attractors can be of relevance - for instance, the attractor with frequency synchronization is required for proper operation of power grids, and switching to an undesired attractor may correspond to a blackout.

After introducing the fundamental theoretical concepts used in this thesis (Chapter 2), we move to the first work in the thesis (Chapter 3), which studies networks of Kuramoto oscillators with heterogeneous frequencies, a paradigmatic model for studies on synchronization and dynamics of complex networks. By increasing the strength of the inter-unit coupling and by adjusting the topology of connections in the network, these systems display a transition toward phase synchronization. Further, near this transition the networks become very sensitive to changes in parameters of single components, such that even changes to single units can alter the whole network's dynamics. We say that the networks attain a high dynamical malleability and show that this increase in the malleability is due to two effects: increase in sample-to-sample fluctuations near a phase transition and multistability. This work therefore contributes to our understanding of robustness of complex networks, in particular how their malleability and multistability depend on their topology.

In the second work of this thesis (Chapter 3), we focus deeper on mechanisms for multistability, and investigate a network of diffusively coupled excitable neurons. Individually, a unit has only one attractor, a stable equilibrium. Before reaching this attractor, however, trajectories in the excitability region of the unit's state space must go through long excursions. Although the units separately do not have oscillations, we show that a rich variety of stable oscillations can emerge and coexist in the coupled networks. Two coupled units can already have multiple coexisting attractors, with periodic or quasiperiodic oscillations. Going to ten coupled units many more attractors emerge, including a chaotic attractor. We uncover the bifurcations giving rise to these attractors, and explain the qualitative mechanism behind them. We show that the coupling between the units interacts with the excitability region of their state space and manages to repeatedly reinject them there, where they stay effectively trapped. This

serves as a simple yet powerful mechanism for the creation of multistability in networks, and provides insights into how the topology of networks affects their multistability.

Interestingly, the attractors in the previous case arise due to the interaction with the transient dynamics of the units, in the excitability region. Transient dynamics can also play important roles more broadly. In particular, long-lived transients are an ubiquitous behavior in neural activity. In this context, the third work in this thesis (Chapter 4) provides a general conceptual framework for long-lived transients. Looking at the literature, we argue that long-lived transients are the key concept behind metastability, a term that is often used without a clear definition. We make use of the concept of almost-invariant regions, sets in state space wherein trajectories stay for a long time before leaving, and argue that metastable regimes in time correspond to trajectories visiting an almost-invariant region in state space. With this, we identify general dynamical properties of metastability. Then, we discuss many mechanisms that can generate metastability, and provide a classification of subtypes of metastability, which neatly includes previous works in the literature. Our hope is that this framework aids future research in neuroscience, and even other areas in which metastability occurs, such as climate science.

Finally, this thesis also describes a work (Chapter 2.1.7) developing and implementing state-of-the-art algorithms for finding attractors and their basins of attraction, including the possibility to do so in a continuation scenario over a parameter range. These algorithms were used throughout the thesis, and are available in an efficient open-source package for studying dynamical systems.

Zusammenfassung

Chapter 1

Methodology

1.1 Basics of dynamical systems theory

1.1.1 Dynamical systems and the uniqueness and existence of their solutions

In this thesis we study dynamical systems described by a state variable $x = (x_1, x_2, \dots, x_n)^T \in M$, where $M \subseteq \mathbb{R}^n$ is the state space, and T denotes the transpose operation. The state variable is a point in this n -dimensional state space. In a continuous-time dynamical system, the state evolves according to the equation:

$$\dot{x}(t) = f(x(t)) \quad (1.1)$$

where $f : M \rightarrow M$. Systems obeying Eq. 1.1 are deterministic: there is no randomness, no stochasticity, no noise. This means that, starting from one single state at time t , we can in principle describe the whole past and future evolution of the system. Furthermore, there is a lack of an explicit time dependence in f - i.e., $\partial f_i / \partial t = 0$ for $i = 1, \dots, n$. In this case, the dynamical system is said to be autonomous.

To obtain solutions to system 1.1 we need to provide one state, which we typically call an initial condition $x_0 = x(0) \in \mathbb{R}^n$. The combination of $\dot{x} = f(x)$ with $x(0) = x_0$ defines an initial value problem. A fundamental theorem makes our lives studying this problem much easier. This is the theorem of existence and uniqueness of solutions. For $x \in \mathbb{R}^n$ and $f : \mathbb{R}^n \rightarrow \mathbb{R}^n$, it requires that f is continuous and that all of its partial derivatives $\frac{\partial f_i}{\partial x_j}$, for $i, j = 1 \dots n$ are continuous in some open connected set $D \subset \mathbb{R}^n$. This basically means that it requires our function f to be sufficiently smooth. Then, for initial conditions $x_0 \in D$, the initial value problem has a solution $x(t)$ on some time interval $(-\tau, \tau)$ about $t = 0$, and the solution is unique! [1]

In state space, each solution describes a trajectory, a path, that goes through its initial condition x_0 . The uniqueness of solutions implies that, within this time interval $(-\tau, \tau)$, different trajectories do not intersect in state space. This is a crucial property underlying all systems we study.

A useful notation for the evolution of a continuous dynamical system is through the evolution operator $\Phi^t(x)$, which, informally defined, evolves the point x forward t time units. That is, $\Phi^t(x(0)) = x(t)$.

1.1.2 The fate of linear dynamical systems

Although trajectories do not cross, they can share the same fate, meaning they can converge to the region in state space. We can introduce this notion with a very simple mathematical example of a linear system. It has the form

$$\dot{x}(t) = Ax(t) \quad (1.2)$$

where A is a constant $(n \times n)$ matrix.

If the eigenvalues $\lambda_i \in \mathbb{C}$ of A are all unique, its eigenvectors $v_i \in \mathbb{R}^n$ are linearly independent. Then, the general solution to this system can be written as Ref. [1]:

$$x(t) = \sum_{i=1}^n C_i e^{\lambda_i t} v_i. \quad (1.3)$$

Then, each initial condition determines the constant coefficients $C_i \in \mathbb{R}$. From Eq. 1.3 we can already notice that the origin of the system, $o = (0, \dots, 0)^T$, is a solution. In fact, it is an equilibrium: $\dot{x} = f(o) = 0$. A trajectory on the origin does not change over time.

As we see from Eq. 1.3, the behavior of trajectories depends on the eigenvalues λ_i of the matrix A . We can classify the equilibrium at the origin based on these eigenvalues, as shown in Fig. 1.1. If the real parts of all the eigenvalues are negative, then all trajectories in state space converge to the origin as $t \rightarrow \infty$. In this case, the origin is said to be a stable equilibrium (Figs. 1.1A-B). If at least one eigenvalue is negative, the trajectories diverge from the origin, which is then an unstable equilibrium (Figs. 1.1C-E). Stability here refers to the behavior of trajectories near the equilibrium. If it is stable, nearby trajectories converge to the equilibrium - or, equivalently, small perturbations that take a trajectory away from the equilibrium will eventually go back to the equilibrium. If it is unstable, then nearby trajectories diverge from it.

Stable equilibria are the only attracting solution, or attractor, of linear systems. In this case, although different trajectories cannot not intersect, they all converge to the origin as $t \rightarrow \infty$. In summary, the ultimate fate of linear systems is kind of boring: either trajectories end up at the origin or they diverge off to infinity. But the journey, the path that trajectories take before before the end, the *transient dynamics*, is more interesting. As shown in Fig. 1.1, this is dictated by the constellation of eigenvalues λ_i . For more details, the reader can refer to standard books on linear/nonlinear dynamics, such as Ref. [1].

1.1.3 The fate of nonlinear dynamical systems I: attractors

As just seen, stable equilibria are the only possible attractors in linear systems. Going beyond Eq. 1.2, nonlinear systems can have more interesting and complicated long-term dynamics (Fig. 1.2). Stable equilibria are still possible, as shown in Figs. 1.2A-B. The system here is a conductance-based neuronal model following equations [2]

$$\begin{aligned} \dot{x} &= (I - g_L(x_i - E_L) - g_{Na}m_\infty(x_i)(x_i - E_{Na}) - g_Ky_i(x_i - E_K))/C, \\ \dot{y} &= (n_\infty(x) - y_i)/\tau, \end{aligned} \quad (1.4)$$

with all parameters and functions defined in detail in Chapter ???. The input current I is chosen to be $I = 2.0$ so the system has excitable dynamics. Its state space is composed of a stable equilibrium, the only attractor, and two unstable equilibria, which create excitable dynamics. Excitability is a type of transient different than seen for linear systems. Some trajectories are forced to go on long excursions (excitations) before converging to the stable equilibrium. We study more about this again in Chapter ??.

Besides equilibria, nonlinear systems can also have periodic solutions. These orbits vary in time with a certain period T (Fig. 1.2C) and correspond to closed curves in state space (Fig. 1.2). In several cases these periodic solutions are isolated, in the sense that there are no other periodic orbits in some neighborhood around them. In that case, they

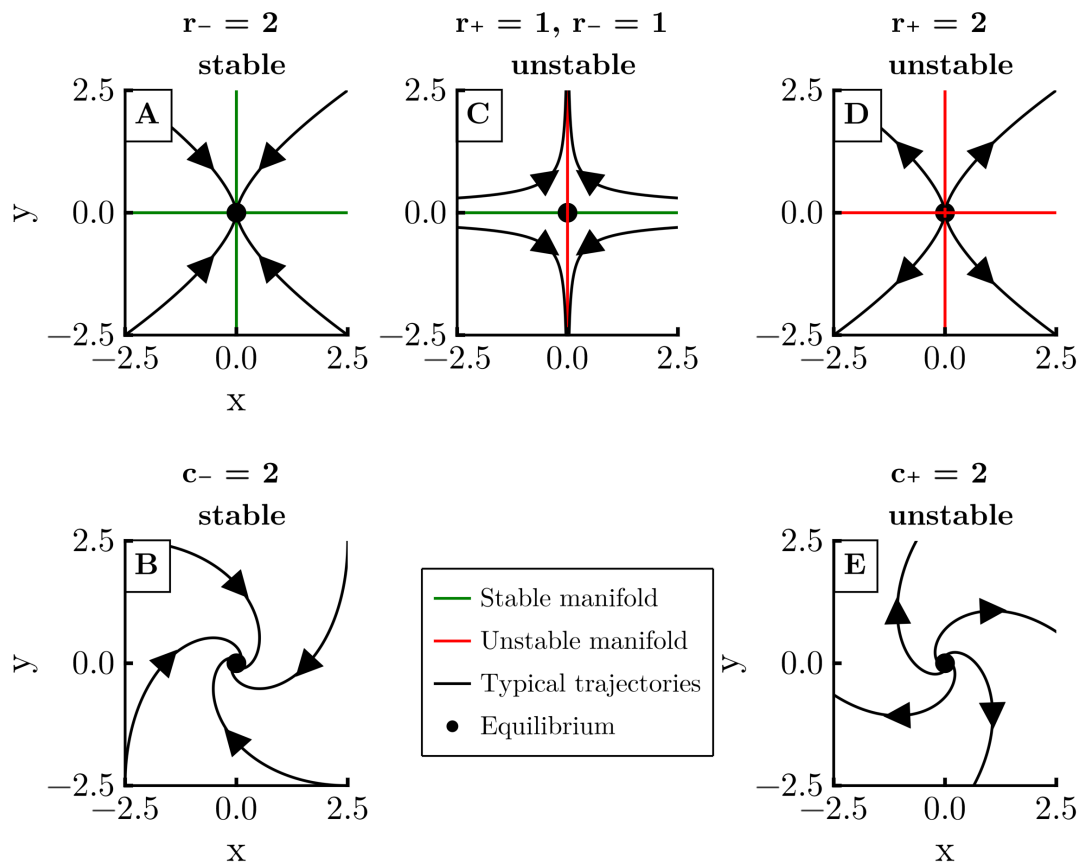


Figure 1.1: **Hyperbolic equilibria in 2D linear systems.** The title specifies the number of eigenvalues that are purely real negative r_- or positive r_+ , or that are complex with real part negative c_- or positive c_+ . The first row shows equilibria whose eigenvalues are purely real, while the second one shows equilibria with complex eigenvalues. In the first column, the equilibria are stable - they are the two possible attractors in linear systems. In the second column, we have a saddle-point for purely real eigenvalues. In the third column, the equilibria are completely unstable, known as repellers.

are called limit cycles. The system used in this example is still the neuronal model of Eq.1.4, but with a different parameter $I = 6$, which leads to the system now having a stable limit cycle. We see in this figure again an example of a long transient, with the trajectory initially going on a long excursion before converging to the limit cycle.

Not all curves in state space are closed, however. One can have quasiperiodic dynamics, in which trajectories never repeat exactly, although they might almost repeat. This is seen in Figs. 1.2E-F. Simulating the trajectory for longer times would fill up the figure more and more. Further, note the varying amplitude of the time series. The system in this example is the forced Van der Pol oscillator,

$$\dot{x} = v \quad (1.5)$$

$$\dot{v} = \mu(1 - x^2)v - \alpha x + g \cos(\omega_f t),, \quad (1.6)$$

with parameters $\mu = 0.1$, $\alpha = 1.0$, $g = 0.5$, $\omega_f = \sqrt{3}$ taken from Ref.[3].

Finally, one can also have chaotic attractors (Figs.1.2G-H). These solutions have a wild behavior that nearby trajectories tend to diverge at an exponential rate [4]. Despite this local divergence, however, the solutions remain bounded in space. In other words, systems with chaotic attractors are very sensitive to the initial conditions - small changes in initial conditions lead to trajectories that can look very different. The system used to generate is shown as the Lorenz system, with equations

$$\dot{x} = \sigma(y - x) \quad (1.7)$$

$$\dot{y} = x(\rho - z) - y \quad (1.8)$$

$$\dot{z} = x * y - \beta * z, \quad (1.9)$$

and $\sigma = 10$, $\rho = 28$, $\beta = 8/3$. This chaotic attractor in particular has a shape that resembles a butterfly, with trajectories spending some time on one wing before switching to the other wing [4].

Given now these examples, let us now define the terms we have used a bit more properly.

1.1.4 Formalizing attractors and basins

We have just presented examples of attractors, sets of points in state space to which trajectories eventually converge, and their basins of attraction, the regions containing those converging trajectories. Since in this thesis we will deal a lot with these concepts, we provide now an attempt at formalizing. The idea is to have the concepts clear in mind for later. In practice, we will only use the informal definition we just gave. In particular, the definition of attractor can vary considerably in the literature. Without attempting to claim any superiority, we attempt here to provide a definition that suits our studies.

First, we define an omega limit set $\omega(x)$ of a point $x_0 \in M$ as [5]:

$$\omega(x_0) = \{x : \forall T \forall \epsilon > 0 \text{ there exists } t > T \text{ such that } |f(x_0, t) - x| < \epsilon\}. \quad (1.10)$$

Consider a point $x \in \omega(x_0)$ in the ω limit set of x_0 . Then, by definition, a trajectory that passes through x_0 comes arbitrarily close to x infinitely often as t increases.

From this, we can define the *basin of attraction* of a set A as $\mathcal{B}(A) = \{x \in M : \omega(x) \subset A\}$. This only looks at the long-term behavior of trajectories; the transient

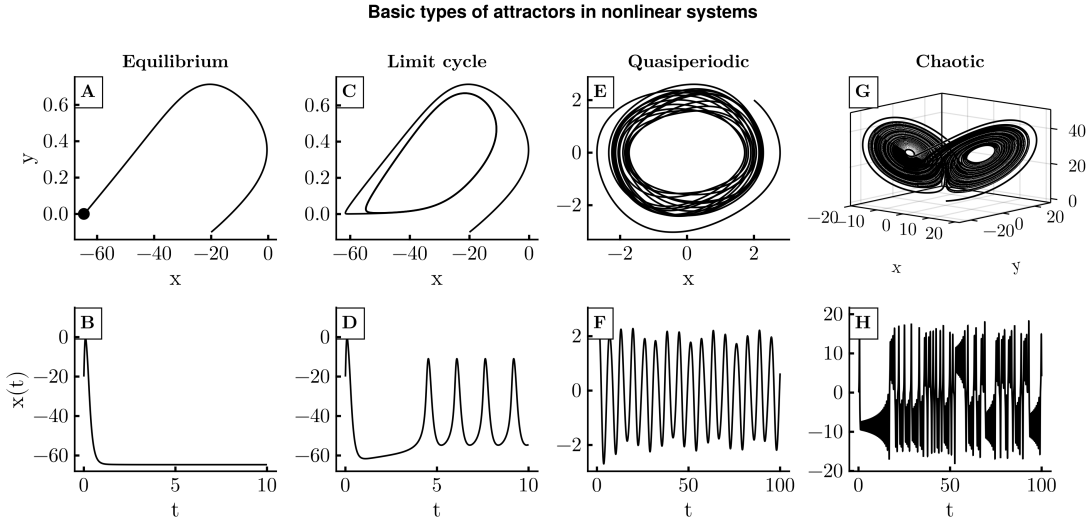


Figure 1.2: **Basic types of attractors in nonlinear dynamical systems.** Each column shows respectively the state space and a time-series of a typical trajectory converging to a type of attractor. The first column corresponds to the neuronal model of Eq.1.4 with $I = 2.0$, which has excitable dynamics, converging to a stable equilibrium. The second column shows again the neuronal system of Eq.1.4 but with $I = 6.0$, when the attractor is now a stable limit cycle. The third column shows the system defined in Eqs.1.6, with a quasiperiodic attractor. Finally, column four has an example of a chaotic trajectory on the Lorenz system (Eq. 1.9).

dynamics could be anything, including the case that trajectories go very far from A , as long as they go back to it and stay there eventually.

Now to define an attractor, we first define a weaker (or, on the more optimistic side, a more general) version, called the *Milnor attractor*. It is a useful concept when dealing with metastability. A set A is a Milnor attractor if:

1. Its basin of attraction $\mathcal{B}(A)$ has strictly positive measure (i.e., if $m(\mathcal{B}(A)) > 0$), where $m(S)$ denotes a measure equivalent to the Lebesgue measure of set S [5]. This condition says that there is some probability that a randomly chosen point will be attracted to A [5].
2. For any closed proper subset $A' \subset A$, the set difference $\mathcal{B}(A) \setminus \mathcal{B}(A')$ also has strictly positive measure. This ensures that every part of A plays an essential role - one cannot decompose A into an attracting part and another part that does not attract [5, 6]. A closed set here means that it contains all its limit points. And proper means its non-empty.

Furthermore, the Milnor attractor does not have to attract all the points in its neighborhood, and there can also be orbits that transiently go very far from the attractor, even if initially close, before eventually getting close to it. Further, it can in principle be composed into the union of two smaller Milnor attractors. To avoid these cases, we call a set A an *attractor* if

1. A is a Milnor attractor.

2. A contains an orbit that is dense in A . Basically, this means that there is an orbit in A that passes arbitrarily close to every point in A . This condition ensures that the attractor is not the union of two smaller attracting sets [6].
3. There are arbitrarily small neighborhoods U of A such that $\forall x \in U$ one has $\Phi^t(x) \subset U \forall t > 0$ and such that $\forall y \in U$ one has $\omega(y) \subset \omega(x)$. That is, there are arbitrarily small neighborhoods around the attractor in which points inside stay inside and converge to A . This criterion is given in Ref. [7].

1.1.5 Invariant manifolds: structures that organize state space

In Sec. 1.1.2 we only considered the case when all the eigenvalues of the matrix A in the linear system $\dot{x} = Ax$ were positive. If one eigenvalue λ_k is positive, then trajectories will diverge to infinity following the corresponding eigenvector v_k . When some eigenvalues are positive, and some are negative, the origin is a saddle-point. If all eigenvalues are positive, it is called a repeller. Figure 1.1 shows examples of equilibria in 2D linear systems. Note that typical trajectories approach the saddle-point along the y -axis and then diverge along the x -axis. That is, for $t \rightarrow -\infty$, trajectories converge to the y -axis and for $t \rightarrow \infty$ they converge to the x -axis. The y -axis is called the stable manifold $\mathbb{W}^s(o)$ of the origin o and the x -axis is the unstable manifold $\mathbb{W}^u(o)$ of the origin. We can define these manifolds

$$\mathbb{W}^s(o) = \{x \in M : \Phi^t(x) \rightarrow o \text{ as } t \rightarrow \infty\}, \quad \mathbb{W}^u(o) = \{x \in M : \Phi^t(x) \rightarrow o \text{ as } t \rightarrow -\infty\}. \quad (1.11)$$

Let us separate the eigenvectors v_i into two parts: the ones with negative eigenvalues $v_1^-, \dots, v_{n_s}^-$ and the ones with positive eigenvalues $v_1^+, \dots, v_{n_u}^+$. Then we can define the stable and unstable subspaces, respectively, as

$$\mathbb{E}^s = \text{span}(v_1^-, \dots, v_{n_s}^-) \quad \mathbb{E}^u = \text{span}(v_1^+, \dots, v_{n_u}^+) \quad (1.12)$$

For a linear system, the stable manifold of the origin coincides with the stable space \mathbb{E}^s and the unstable manifold coincides with the unstable space. In general, as in the example of the saddle-point, these manifolds act to organize the behavior of trajectories in state space.

These concepts can be extended for nonlinear systems. To do this, the first step is to think about the linearization of the nonlinear system. Suppose our nonlinear system of interest has an equilibrium $x^* \in M$. It turns out that the behavior sufficiently close to this equilibrium is linear, despite the system globally being nonlinear [8, 9]! To see this, we first move the origin of our system to x^* by defining a new variable $y(t) = x(t) - x^*$. Then,

$$\dot{y} = \dot{x} = f(y + x^*) \equiv g(y) \quad (1.13)$$

where we define a convenience function $g(y)$. Expanding $g(y)$ around $y = 0$ (i.e., around the equilibrium $x(t) = x^*$) gives us

$$\dot{y} = g(0) + J_g(0)y + \mathcal{O}(y^2), \quad (1.14)$$

where $J_g(y) = \frac{\partial g_i(y)}{\partial y_j}$ is the Jacobian of g . It is related to the Jacobian of f by $J_g(y) = J_f(x)$, so $J_g(y=0) = J_f(x=x^*)$. Since $g(0) = f(x^*) = 0$, then if we are

sufficiently close to the origin we can also ignore the terms $\mathcal{O}(y^2)$ and therefore we get

$$\dot{y} = J_g(0)y. \quad (1.15)$$

That is, the behavior of the nonlinear system sufficiently close to the equilibrium is linear, with the constant matrix function being the Jacobian evaluated at the equilibrium!

But the good news don't stop here! There is the Hartman-Grobman theorem, which basically shows that the state space near a hyperbolic equilibrium to the state space of the linearization. An equilibrium is hyperbolic if the eigenvalues of the Jacobian evaluated on it are all nonzero, i.e., if $\lambda_i \neq 0 \forall i = 1, \dots, n$. *Topologically equivalent* means that the linearized state space and the local state space near the equilibrium are distorted versions of each other. They can be bended and warped, but not ripped. In particular, closed orbits have to remain closed, and connections between saddle points have to remain [1]. Mathematically, topologically equivalent means there is a *homeomorphism* (continuous deformation with continuous inverse) from one state space into the other; trajectories can be mapped from one to the other, and the direction of time is the same [1].

Stating the theorem more formally, suppose a hyperbolic equilibrium $x^* \in M$ such that $f(x^*) = 0$ and such that all its eigenvalues are nonzero. Then, there is a neighborhood N of x^* and a homeomorphism $h : N \rightarrow M$ such that [4]

- $h(x^*) = 0$
- the flow $\dot{x} = f(x)$ in N is topologically conjugate to the flow of the linearization $\dot{y} = Ay$ by the continuous map $y = h(x)$. Topologically conjugate basically meaning a change of coordinates in a topological sense.

This guarantees that the stability of the equilibrium is the same in both cases, so we can use the linearization to gain important insights about the stability of equilibria in the nonlinear system!

What about the stable and unstable manifolds? In analogy to the linear case, we can define local stable and unstable sets near a neighborhood U of an equilibrium x^* for the nonlinear system [4]:

$$\mathbb{W}_{\text{loc}}^s(x^*) = \{x \in M : \Phi^t(x) \rightarrow o \text{ as } t \rightarrow +\infty \text{ and } \Phi^t(x) \in U \forall t \geq 0\}, \quad (1.16)$$

$$\mathbb{W}_{\text{loc}}^u(x^*) = \{x \in M : \Phi^t(x) \rightarrow o \text{ as } t \rightarrow -\infty \text{ and } \Phi^t(x) \in U \forall t \leq 0\}. \quad (1.17)$$

Herein comes the stable manifold theorem. It states that, for a hyperbolic equilibrium x^* :

- The local stable set $\mathbb{W}_{\text{loc}}^s(x^*)$ is a smooth manifold whose tangent space has the same dimension n_s as the stable space \mathbb{E}^s of the linearization of f at x^* . $\mathbb{W}_{\text{loc}}^s(x^*)$ is also tangent to \mathbb{E}^s at x^* .
- The local unstable set $\mathbb{W}_{\text{loc}}^u(x^*)$ is a smooth manifold whose tangent space has the same dimension n_u as the unstable space \mathbb{E}^u of the linearization of f at x^* . $\mathbb{W}_{\text{loc}}^u(x^*)$ is also tangent to \mathbb{E}^u at x^* .

The homeomorphism guaranteed by the Hartman-Grobman theorem maps $\mathbb{W}_{\text{loc}}^s(x^*)$ into \mathbb{E}^s and $\mathbb{W}_{\text{loc}}^u(x^*)$ into \mathbb{E}^u one-to-one, as shown in Fig. XX. Further, the stable manifold theorem guarantees that \mathbb{E}^s and \mathbb{E}^u actually approximate the local manifolds

$\mathbb{W}_{\text{loc}}^s(x^*)$ and $\mathbb{W}_{\text{loc}}^u(x^*)$, respectively [4]. As a consequence, we get the behavior illustrated in Fig. 1.3

The manifolds we just looked at are defined for a local neighborhood U around the equilibrium. We can extend them towards the whole of state space by defining global manifolds as:

$$\mathbb{W}^s(x^*) = \bigcup_{t \leq 0} \Phi^t(\mathbb{W}_{\text{loc}}^s(x^*)) \quad (1.18)$$

$$\mathbb{W}^u(x^*) = \bigcup_{t \geq 0} \Phi^t(\mathbb{W}_{\text{loc}}^u(x^*)) \quad (1.19)$$

That is, the global stable manifold is obtained by integrating the local stable manifold backwards, looking at where the trajectories on it came from. For the unstable manifold, we integrate the local unstable manifold forwards, to see where it goes to.

An important fact about the local and global manifolds that follows from their definitions is that they are invariant: trajectories starting on these manifolds stay on them forever [4]. Furthermore, the uniqueness of solutions prohibits certain crossings of manifolds: stable manifolds of two distinct equilibria cannot cross, unstable manifolds of two distinct equilibria also cannot, and the same manifold cannot cross itself - otherwise, where the crossing points would have to obey two distinct paths! Meanwhile, stable and unstable manifolds, either of the same equilibrium or of two different equilibria can cross.

As mentioned before, these manifolds usually play a big role in organizing state space. As we will see in Chapter ??, they can organize the transient dynamics of systems. There, we study a dynamical system wherein certain trajectories are forced to go on long excursions before converging to the stable equilibrium, the only attractor in state space (see Figs.1.2A-B). As explained there, this long excursion is generated by the arrangement of the invariant manifolds of the saddle-point that exists in state space. The invariant manifolds can also organize the long-term behavior of systems: the next section briefly shows how stable manifolds of unstable equilibria can act as the boundary separating two basins of attraction.

1.1.6 The fate of nonlinear dynamical systems II: multistability and basins of attraction

In Sec. 1.1.3 we saw that the ultimate fate of nonlinear systems, their attractors, can be much more complicated than that of linear ones. Not only are the attractors themselves complicated, but they can also coexist in state space. If there are two coexisting attractors, this means that the state space will be separated into three regions: the basin of attraction of attractor one, the basin of attractor two, and the boundary between them. Usually, the basin boundary is formed by stable manifolds of saddle-type objects: saddle-points, saddle-limit-cycles, and even chaotic saddles! [10]. Figure 1.4 illustrates this for a relatively simple system with two stable equilibria, where the basin boundary is the stable manifold of the saddle-point in the middle. This system is known as the Duffing oscillator:

$$\dot{x} = v \quad (1.20)$$

$$\dot{v} = -(-kx + cv + lx^3)/m, \quad (1.21)$$

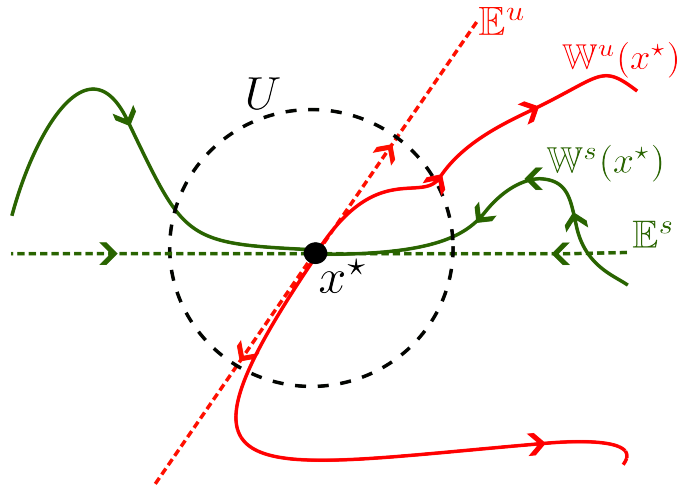


Figure 1.3: **Invariant manifolds of saddle point x^* .** The local stable $W_{\text{loc}}^s(x^*)$ and unstable $W_{\text{loc}}^u(x^*)$ manifolds of the saddle point x^* respectively can be associated with the stable E^s and unstable E^u subspaces and become tangent to them near the saddle. This follows from the Hartman-Grobman and the stable manifold theorems. The global stable $W^s(x^*)$ and unstable $W^u(x^*)$ manifolds extend the definition of the local manifolds beyond the neighborhood U . Figure is inspired by Fig. 6.2.4 from Ref. [4].

with $k = 1$, $c = 0.5$, $l = 1$, $m = 1$. This system represents a ball of mass m rolling downhill at position x and velocity v on a quartic potential landscape of the form $U(x) = -lx^4/4 - kx^2/2$ with a friction term $-cv$. Following the definition of global manifolds in Eq. 1.19, these global manifolds are essentially obtained by integrating trajectories starting on the local manifolds of the saddle-point.

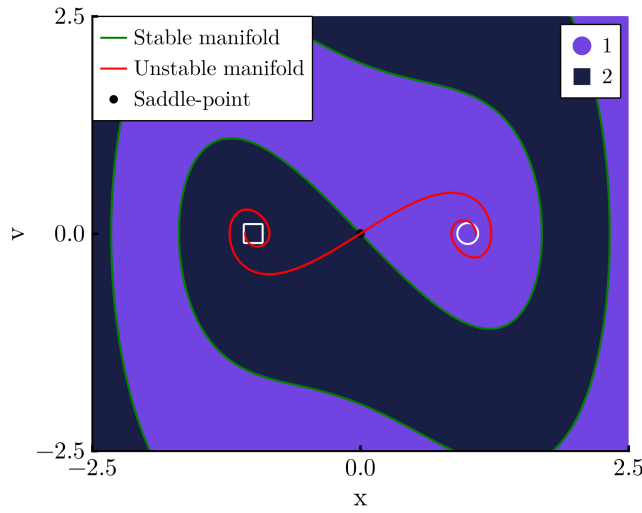


Figure 1.4: **Bistability in Duffing model.** Two stable equilibria (white square and circle) are shown with their respective basins of attraction in two shades of purple. The global stable and unstable manifolds of the saddle-point (black point) in the middle are also shown as green and red lines respectively. The global stable manifold of the saddle coincides with the boundary between the basins.

In this thesis we study two examples of multistability occurring in networked systems. In Chapter 2 we study networks of Kuramoto units, and see there the coexistence of multiple attractors depending on how strongly the units are interacting. We also see how this multistability impacts the sensitivity of the system to small changes in parameters of the units. Later, in Chapter ?? we study how multistability arises when two excitable neurons are coupled together diffusively. Both studies require that we find the attractors in the systems. This is what we deal with in the next section.

1.1.7 How to find attractors

Finding all the attractors of a given dynamical system is not necessarily a trivial task. For equilibria, one can find all the roots of the system function, i.e., $f(x^*) = 0$ and then check their stability through the eigenvalues of the Jacobian evaluated on them. However, the problem becomes more complicated for other types of attractors. To start off, simply proving that a set is an attractor, following the criteria given in Sec. 1.1.4, is usually not possible. Instead, in practice we use the looser definition of an attractor simply as the long-term dynamics of trajectories. Numerically, this means a brute-force approach of simulating several trajectories in state space for long integration times and seeing where they converge to.

This comes with two problems. First, it does not rule out the possibility that a certain set is just a very long transient. To remedy this, we usually integrate trajectories on the set for very long and check if there is any escape. Second, some attractors might have very small basins of attraction, such that randomly chosen initial conditions are unlikely to end on them, so it is unlikely that we find those attractors. So far, however, this brute force approach is the best we have for general systems [11, 12]. Within this approach, there are two main methods in the literature for finding attractors. They differ in how they check convergence to attractors.

The first approach was proposed in Ref. [13] and implemented with improvements in Ref. [11]. It parcellates state space into boxes. The idea then is that a typical trajectory, initialized in a certain box in state space, will evolve and visit other boxes until it converges to the attractor. It will then stay on the attractor, repeatedly visiting the same state space boxes. Using this idea, the algorithm integrates trajectories and looks for recurrences. When boxes are visited repeatedly for a certain prescribed amount of time, the algorithm considers that these boxes constitute the attractor. It is also smart in that it keeps track of the state of each box. So it knows that the boxes visited by the trajectory before converging to the attractor - the transient section of the trajectory - belongs to the basin of attraction of that attractor. This algorithm works well for steady-state, periodic, quasiperiodic, and chaotic attractors in low-dimensional systems. For chaotic attractors in high-dimensional systems it does not work well, because the time that trajectories take to recur on a chaotic attractor becomes too long to simulate numerically.

The second method does not rely on discretizing state space, and is designed to work well for high-dimensional systems. In this case, one spreads a number \mathcal{N} of initial conditions in state space and integrates them to obtain \mathcal{N} trajectories. Each trajectory $x(t)$ is then converted to a vector of features $\mathcal{F} \in \mathbb{R}^n$ of n numbers that all collectively describe the trajectory. This is done by the featurizing function $\phi : M \times \mathbb{R} \rightarrow \mathbb{R}^n$, such that $\mathcal{F} = \phi(x(t), t)$. Each attractor should correspond to a unique \mathcal{F} . Then, the \mathcal{N} vectors of features are grouped together via any of several possible grouping or clustering

algorithms, and each grouping corresponds to one attractor. This approach can work very well, but it relies on pre-existing knowledge about the system to find a suitable featurizer function ϕ . To be confident about the results, one also has to verify that the total integration time is long enough, and that the transients of all trajectories were removed. This relies on experimentation. This method has been proposed in Ref. [14] and soon thereafter also in Ref. [15]. Together with colleagues, I implemented efficient and open-source code for this method with improvements in the Attractors.jl package Ref. [12].

Both methods can be applied across a parameter range and used in a continuation fashion, as illustrated in Fig. 1.1.7A. For the first parameter, one selects \mathcal{N} initial conditions and identifies from those the attractors of the system using any of the two methods just described. Then, one samples points on these attractors and adds them to the pool of initial conditions for the next parameter value. The originally prescribed initial conditions, together with the original ones, are then used to find attractors in the subsequent parameter value. This process of seeding initial conditions from the previously found attractors is repeated for the whole parameter range. Then, one has all the attractors for each parameter value, and the remaining problem is to link attractors from one parameter to the next.

The matching procedure between attractors is crucial for a continuation procedure. Often in linear continuation analysis one just matches the next point along a continuation curve to the previous point. This works well for infinitesimal perturbations of fixed points but becomes a problem in global stability analysis, where the steps are not necessarily infinitesimal and the attractors may be spatially extended and chaotic. Matching in our algorithm is designed to be very flexible, and can be adapted to the user's needs [12]. First, the algorithm computes the distances between attractors at some parameter p_i and some subsequent parameter p_{i+1} . Distance here is any positive semi-definite function. The default used is the Euclidean distance between the centroids of the attractors. Another good option is the Hausdorff [12]. With the distances, a new attractor is matched to the previous one with the smallest distance, prioritizing pairs with the smallest distance. This matching respects uniqueness, so that once an attractor from the previous parameter has been matched, it is removed from the matching pool.

After matching, the continuation is done. The user may also decide to group attractors based on some features of interest. For instance, to group attractors with a certain degree of synchronization [12].

The development and implementation of the attractor-finding algorithms and the continuation procedure in efficient and open-source code led to a joining publication in Ref. [12].

1.2 Basics of bifurcations

What happens to the attractors - and, in general, to the state space structures - of a dynamical system when we vary its parameters? In terms of the qualitative properties, there are two possibilities: either they stay similar or they change drastically. We can be a bit more rigorous. Two systems are qualitatively similar if they are topologically equivalent. The notion of topological equivalence was already mentioned in Sec. 1.1.5. As a reminder, two systems are topologically equivalent if the state space of one can be obtained by a continuous transformation of the other [16]. Mathematically, this means that they are topologically equivalent if there is a homeomorphism $h : M \rightarrow M$ mapping

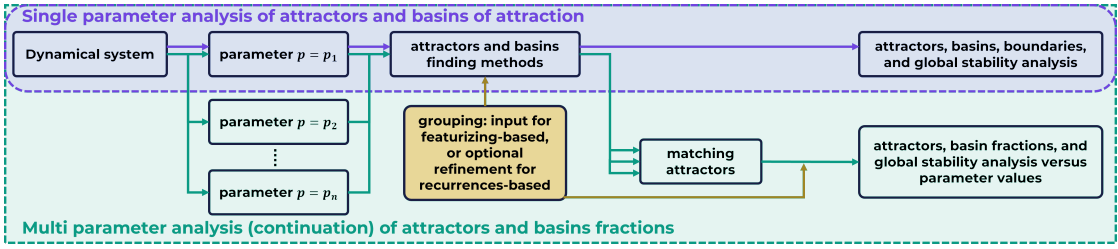


Figure 1.5: **Schematic illustration of the continuation method used to find and match attractors across a parameter range.** The first row illustrates the single-parameter attractor finding algorithms. The second row illustrates how they can be combined across parameters to perform a continuation analysis. Figure taken from Ref. [12].

orbits of the first system onto orbits of the second, preserving the direction of time.

As the parameters of a system are varied, we obtain different dynamical systems that are usually topologically equivalent. The attractors, for instance, may move, but they retain their stability. At some point, however, there may be a drastic change, and the new system may no longer be equivalent. The attractor may have disappeared, or lost its stability. Or a new attractor may have emerged. These drastic qualitative changes in the behavior of a dynamical system are called bifurcations. A bit more rigorously, a bifurcation is a change in the topological type of a system as its parameters pass through a critical (bifurcation) value [16]. There are many different types of bifurcations, and one can literally write a whole book about this [16]. For this thesis we focus briefly on just a few bifurcations that will be relevant for later. For simplicity, we focus also on the simplest version of these bifurcations.

1.2.1 Saddle-node bifurcation of equilibria

In a saddle-node bifurcation of equilibria we see the emergence, or destruction, of a stable (node) and an unstable (saddle) equilibrium. Starting from the side of the bifurcation in which the equilibria exist and approaching the bifurcation parameter, we see the equilibria approaching each other, coalescing at the critical parameter, and annihilating each other thereafter. The simplest form of this bifurcation occurs in one dimension in the system

$$\dot{x} = f(x) = \alpha + x^2, \quad (1.22)$$

with the critical value of the bifurcation being $\alpha = 0$. As shown in Figs. 1.6, for $\alpha < 0$ we see that the parabola $f(x)$ has two roots, so the system has two equilibria, in positions $x^* = \pm\sqrt{-\alpha}$. From the figure directly we can already see that the equilibrium on the left is stable and the equilibrium on right is unstable. We can confirm this with a linearization analysis - the Jacobian here is simply $df/dx = 2x$, so the eigenvalue of the left and right equilibrium are $-2\sqrt{-\alpha}$ and $+2\sqrt{-\alpha}$. As α increases towards 0 the parabola moves up, the equilibria approach each other, their eigenvalues approach zero, and at $\alpha = 0$ they all coalesce into one single equilibrium. At this point, the eigenvalue of the system is zero: this equilibrium is non-hyperbolic! For $\alpha > 0$ there are no more equilibria. Equation 1.22 is called the normal form of the saddle-node bifurcation, because any

generic system obeying some conditions will be topologically equivalent to it locally, near the equilibrium. For a system $\dot{x} = f(x, p)$, with $x \in \mathbb{R}$ and $\alpha \in \mathbb{R}$, $\partial f(0, 0)/\partial x = 0$, an equilibrium $x = 0$ at the critical parameter $\alpha = 0$, the conditions are [16]:

$$\frac{\partial^2 f(0, 0)}{\partial x^2} \neq 0 \quad (1.23)$$

$$\frac{\partial f(0, 0)}{\partial \alpha} \neq 0. \quad (1.24)$$

They guarantee that the system $\dot{x} = f(x, p)$ can be transformed into Eq. 1.22 or into $\dot{x} = \alpha - x^2$, which just inverts the direction of α .

After the two equilibria are destroyed, the system does not have an Just after the bifurcation, the region previously occupied by the two equilibria is still quite slow. Note how \dot{x} is very close to zero near $x = 0$ in Fig.1.6. This region of slow flow is called the ghost of the saddle-node [1]. In a way, it retains properties of the two equilibria - particular, trajectories still flow towards the ghost from the side previously occupied by the stable equilibrium, remain in its neighborhood for a while, but then eventually depart through the side previously occupied by the unstable equilibrium [17]. The ghost is not an invariant set, but is an example of a metastable regime, which we study in greater depth in Chapter ??.

Saddle-node bifurcations can also occur analogously for periodic orbits [16] - a stable limit cycle then collides with an unstable limit cycle, and leave behind a ghost of a limit cycle!

1.2.2 Hopf bifurcation

Keeping with the spirit of describing the simplest cases, let us now imagine a system written in polar coordinates (ρ, θ) :

$$\dot{\rho} = f_\rho = \rho(\alpha - \rho^2) \quad (1.25)$$

$$\dot{\phi} = f_\phi = 1. \quad (1.26)$$

Because the two equations are decoupled, we can analyse the ρ equation separately first. First, note that its Jacobian $\partial f_\rho / \partial \rho = \alpha - 3\rho^2$. For all values of α , f_ρ has an equilibrium at $\rho = 0$ - with eigenvalue $\lambda = \alpha$. This is linearly stable for $\alpha < 0$ and linearly stable for $\alpha > 0$. At $\alpha = 0$ it is non-hyperbolic! What happens then? The first equation has another root for $\alpha > 0$ at $\rho = \sqrt{\alpha}$ - so the eigenvalue is $\lambda = -2\alpha$. This equilibrium is unstable for $\alpha < 0$ and stable for $\alpha > 0$. Notice the change of stability of the equilibria: when one is unstable, the other is stable, and vice versa. Considered for f_ρ alone, this is an example of a Pitchfork bifurcation [16]. Considering the full system, with the rotation induced by $\dot{\phi} = 1$, the equilibrium at the origin remains an equilibrium, but the equilibrium at $\sqrt{\alpha}$ becomes a limit cycle with amplitude $\sqrt{\alpha}$. Putting everything together, we have the behavior in Fig. 1.6G-H. A stable limit cycle becomes unstable at $\alpha = 0$ and from it a stable limit cycle emerges. This is called a supercritical Hopf bifurcation [16]. If we write this system in Cartesian coordinates and compute the eigenvalues of the Jacobian at the origin, we see they are $\lambda_{1,2} = \alpha \pm i$. This gives us another general property of this bifurcation: at the critical point, the eigenvalues at the origin cross the imaginary axis.

Now consider the system

$$\dot{\rho} = f_\rho = \rho(\alpha + \rho^2) \quad (1.27)$$

$$\dot{\phi} = f_\phi = 1. \quad (1.28)$$

Now the Jacobian is $\partial f_\rho / \partial \rho = \alpha + 3\rho^2$. There is still an equilibrium at the origin, in which the eigenvalue is still α - its stability is the same as before. However, the other equilibrium, now $\sqrt{-\alpha}$ has the associated eigenvalue as -2α . It therefore exists for $\alpha < 0$ when it is unstable. This thus corresponds to an unstable limit cycle, which coexists with a stable equilibrium for $\alpha < 0$. For $\alpha > 0$, the limit cycle disappears and the system is left with only an unstable equilibrium. This is called a subcritical Hopf bifurcation [16]. The eigenvalues of the Cartesian Jacobian at the origin behave in the same way as for the supercritical Hopf.

1.2.3 Homoclinic bifurcation

Both the saddle-node and the Hopf bifurcations happen in the neighborhood of equilibria - for this reason, they are called local bifurcations. Now we move to a bifurcation in which this is no longer the case - the state space beyond only the equilibrium is affected, and it is thus called a global bifurcation [16]. The formal description of this bifurcation is consequently more involved, and goes beyond the scope of this thesis. For here it is enough to describe the bifurcation more qualitatively.

In the homoclinic bifurcation we study here, occurring on the plane, we have the emergence of a limit cycle. Before the bifurcation, there is only a saddle point. At the bifurcation, the unstable manifold of the saddle becomes tangential to its own stable manifold - this constitutes a homoclinic orbit. After the bifurcation, the homoclinic orbit becomes a limit cycle whose stability depends on the eigenvalues of the saddle. Defining the saddle quantity $\sigma = \lambda_1 + \lambda_2$, it can be shown [16] that the limit cycle is stable for $\sigma < 0$ and unstable if $\sigma > 0$.

Varying the bifurcation parameter α close to the homoclinic orbit, the limit cycle approaches more and more the saddle point, and touches it at $\alpha = \alpha_c$. The region of the limit cycle close to the saddle-point has a very slow dynamics, such that the period of the limit cycle diverges to infinity as the critical point is approached. In higher dimensional systems, different types of homoclinic bifurcations are possible, with potentially much more complicated dynamics. The homoclinic bifurcations we deal with in this thesis are always related to simple saddle points, and so are analogous to the planar case shown now.

An example of a planar system with this bifurcation is due to Sandstede [18]

$$\dot{x} = -x + 2y + x^2 \quad (1.29)$$

$$\dot{y} = (2 - \alpha)x - y - 3x^2 + (3/2)xy. \quad (1.30)$$

The origin is a saddle which, at $\alpha = 0$, has eigenvalues $\lambda_1 = 1$ and $\lambda_2 = -3$ - its saddle quantity is therefore $\sigma = 2 < 0$, so the limit cycle that emerges here is stable [16].

1.3 Basics of network theory

An incredibly powerful abstraction about real-world systems can be achieved through the concept of networks, here used as synonyms for graphs, which are composed of

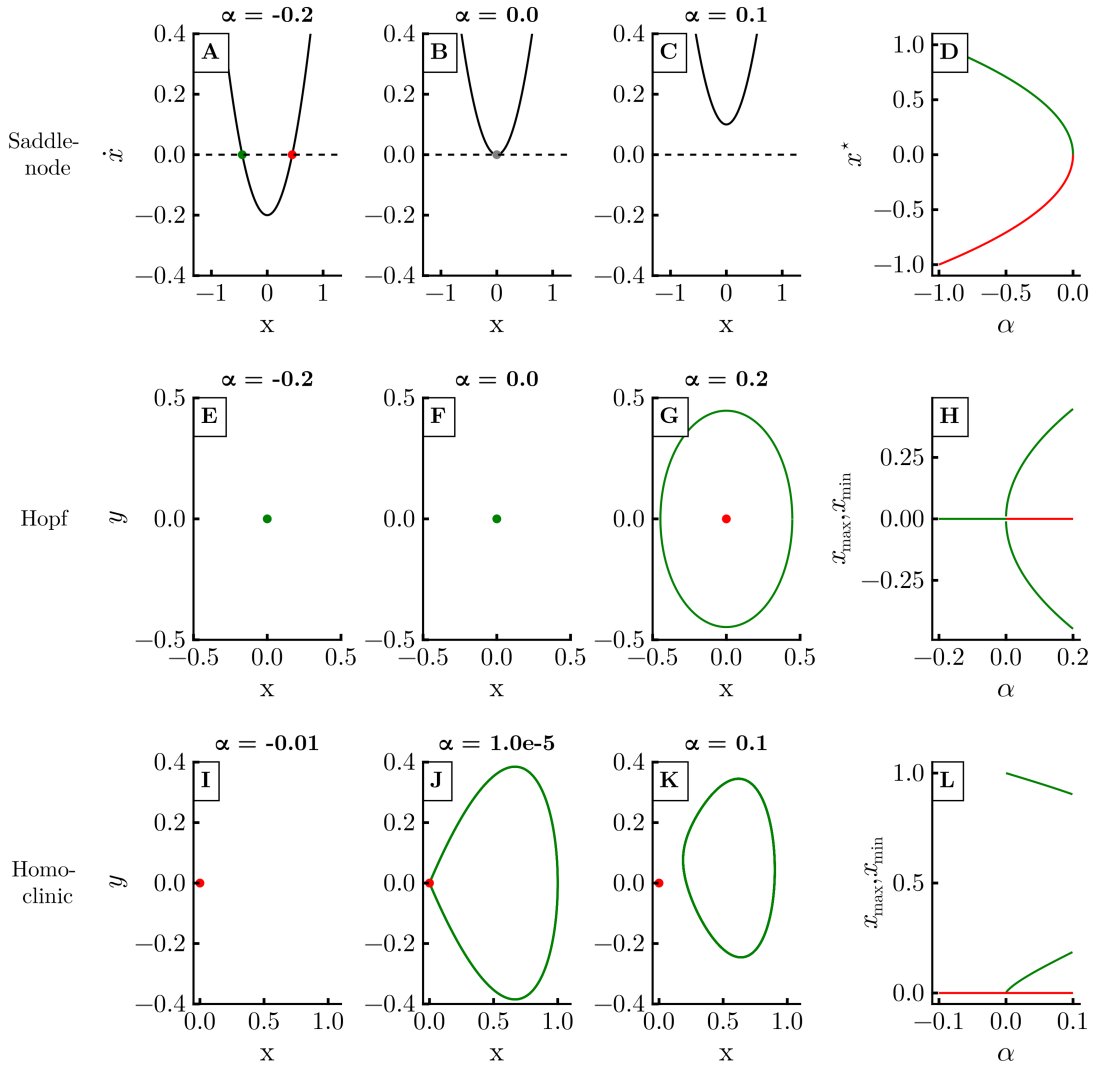


Figure 1.6: Some important bifurcations. The saddle-node bifurcation is shown for the normal form $\dot{x} = x^2 + \alpha$ in panels A-D. A stable and an unstable equilibria, represented respectively by green and red circles (panel A), come together as the bifurcation parameter α is changed. Eventually they coalesce (panel B) and are subsequently destroyed (panel C). The position of these equilibria as a function of α is shown in panel D. The supercritical Hopf bifurcation is shown for Eq. 1.25 in panels E-H. Before and at the bifurcation there is a stable equilibrium in state space (panels E and F respectively), which becomes unstable when a stable limit cycle emerges (panel G). Panel H shows this behavior as a function of α , taking the maximum and minimum values of x to represent the limit cycle. The homoclinic bifurcation to a saddle point is shown in panels I-L. Before the bifurcation there is a saddle point (panel I). At the bifurcation, an orbit homoclinic to this saddle point appears (represented approximately in panel J). After the bifurcation, a stable limit cycle emerges (panel K). This is also summarized in panel L.

nodes that are connected by edges. Networks can represent friendships - with people being the nodes and their friendships being the edges -, brain circuits - neurons are nodes, synapses are edges [19] -, ecological systems - for instance, ecological regions are nodes, and migrations between them are edges [20]. In this thesis we make use of this abstraction and consider that the nodes are dynamical systems $\dot{x}_i = f(x_i)$, $x_i \in \mathbb{R}^n$ on their own, with certain interactions between them. Together, the whole networked system is a dynamical system of the form:

$$\dot{x}_i = f(x_i) + \sum_{j=1}^N A_{ij}g(x_j, x_i), \quad i = 1, \dots, N \quad (1.31)$$

with N units, whose interactions are described by the function g . The adjacency matrix A_{ij} describes the strength of interactions between the units. Typically it is a binary matrix, such that $A_{ij} = 1$ if unit i receives a connection from unit j and $A_{ij} = 0$ otherwise. It can also be weighted, in which case the entry $A_{ij} \in \mathbb{R}$ represents the strength of interactions. Usually for binary matrices, we rewrite Eq. 1.31 as

$$\dot{x}_i = f(x_i) + \sum_{j \in \Omega_i} g(x_j, x_i), \quad i = 1, \dots, N \quad (1.32)$$

where $\Omega_i = \{j \in [1, N] : A_{ij} = 1\}$ is called the neighborhood of unit i . The number of elements in Ω_i , i.e., the number of connections of unit i , is called the unit's degree.

The adjacency matrix A describes the topology of the network, meaning the architecture of the connections. There are many different types of topologies, which describe well different types of systems. One type of topology is the regular, also called k -nearest-neighbors topology. As the name suggests, one can think of all nodes arranged on a ring, with each node connected to the k nearest nodes on each side. Another type of topology is the random topology, in which connections are chosen at random between the nodes. One consider the regular and random topologies as two extremes, and interpolate between them in what is called the Watts-Strogatz algorithm [21]. In this case, one starts with a k -nearest neighbor ring of nodes. Then, choose connections with a probability p . For each chosen connection (i, j) , keep the source node i , randomly choose a new node j' in the network, and switch (i, j) to (i, j') . This effectively switches short-range connections (between nearest nodes) to long range connections (between nodes that are potentially far away). For this rewiring probability p at $p = 0$ one has the regular topology; for $p = 1$ one has the random topology.

Informally speaking, a regular network is considerably clustered, with its short-range structures. And the average distance (in terms of numbers of edges) in the network is considerably high. In a random network, clustering is very small, but the average distance is small. One can formalize these concepts and show how this transition occurs as p is changed [21]. Here, we mention that, when p is relatively small, only a few short-range connections are rewired as long-range. This does not change the clustering characteristics much, but considerably lowers the average distance between nodes - those few long-range connections act as efficient shortcuts between nodes. Networks in this regime are usually called small-world networks [21].

In Chap. 2 we also study distance-dependent networks. The adjacency matrix is then defined as

$$A_{ij} = \frac{1}{\eta(\alpha)(d_{ij})^\alpha}, \quad (1.33)$$

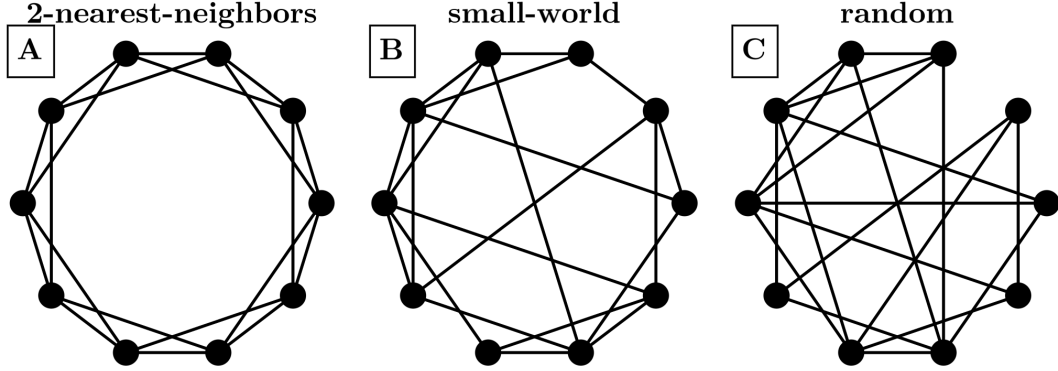


Figure 1.7: **Illustration of networks generated by the Watts-Strogatz procedure.** First, a k -nearest neighbor topology is created (Panel A). Then, some connections are randomly rewired, keeping the source node but changing the target node. With a few rewirings, this creates small-world networks (Panel B). With many rewirings, the network becomes randomly connected (Panel C).

with $d_{ij} = \min(|i - j|, N - |i - j|)$ is the edge distance along the ring, and $\eta(\alpha) = \sum_{j=1}^{N'} \frac{2}{j^\alpha}$ is a normalization term. All units are thus connected, but the weight of the connections decays with the distance following the α parameter. This parameter can also be called the locality parameter, since $\alpha = 0$ leads to an all-to-all equally connected network and $\alpha \rightarrow \infty$ leads to a first-nearest-neighbor topology ($k = 1$). In between we get distance-dependent weights.

1.4 Basics of Kuramoto oscillators

1.4.1 Derivation of the model and transition to synchronization

The Kuramoto model, written in general as

$$\dot{\theta}_i = \omega_i + \epsilon \sum_{j=1}^N A_{ij} \sin(\theta_j - \theta_i) \quad (1.34)$$

serves as a paradigm for studies on synchronization phenomena [22]. Its usefulness comes from it being simple enough to be mathematically tractable, sufficiently generic, and also complex enough to display interesting dynamics. To reach it, Kuramoto started from generic oscillators near supercritical Hopf bifurcations. Each unit i follows

$$\dot{Q}_i = (i\omega + \alpha)Q_i - \beta|Q_i|^2Q_i, \quad (1.35)$$

where ω is the natural frequency of the oscillator, $\alpha > 0$ and $\beta > 0$ are parameters and $Q \in \mathbb{C}$. This is the normal form of the Hopf bifurcation we saw in Sec.1.2 but written in complex numbers. Kuramoto chose a simple and natural way to couple these oscillators: via a common coupling term, that is proportional to the value Q_i of

each oscillator:

$$\dot{Q}_i = (i\omega + \alpha)Q_i - \beta|Q_i|^2Q_i + \frac{K}{N} \sum_{j=1}^N Q_j \quad (1.36)$$

which corresponds to an all-to-all topology, with K being the coupling strength. Here the natural frequencies are assumed to be drawn from a certain distribution $g(\omega)$, usually unimodal.

One can then rewrite (1.36) in polar coordinates by using $Q_i = e^{i\theta_i}\rho_i$. Substituting it one gets the equations

$$\dot{\rho}_i = (\alpha - \beta\rho_i^2) + \frac{K}{N} \sum_{j=1}^N \rho_j \cos(\theta_j - \theta_i) \quad (1.37)$$

$$\dot{\theta}_i = \omega_i + \frac{K}{N} \sum_{j=1}^N \frac{\rho_j}{\rho_i} \sin(\theta_j - \theta_i) \quad (1.38)$$

Kuramoto studied these equations in the limit of $\alpha \rightarrow \infty$ and $\beta \rightarrow \infty$ with α/β constant. Then, one gets that the radial variables ρ_i approach a stable fixed point in arbitrarily fast. The radial variable is therefore just a constant and one just needs to consider the phase variables:

$$\dot{\theta}_i = \omega_i + \frac{K}{N} \sum_{j=1}^N \sin(\theta_j - \theta_i). \quad (1.39)$$

A very useful way to quantify the spread of the phases θ_i is through the complex order parameter:

$$Z = re^{i\psi} = \frac{1}{N} \sum_{j=1}^N e^{i\theta_j}, \quad (1.40)$$

which corresponds to the centroid of the phases and therefore characterizes well the collective behavior of the system. The radius r measures the phase synchronization of the system: r is close to 0 if the phases are uniformly spread or clustered in anti-phase clusters and r is close to 1 if the phases are aligned together. Here we should clarify that phase synchronization denotes the alignment of phases of oscillations - complete phase synchronization corresponds to $r = 1$, meaning that the phases are the same (up to a 2π offsets). On the other hand, frequency synchronization denotes the alignment of the frequencies of oscillations - complete frequency synchronization corresponds to $\dot{\theta}_i = \Omega$, $\forall i = 1, \dots, N$. Networks that are frequency synchronized are also said to be phase-locked - the phase differences are constant. But it does not imply phase synchronization, as the phase differences may be non-zero. Figures 1.8A-B exemplify the behavior of r for weak and strong phase synchronization.

The angle ψ corresponds to the average phase of the units. Using this order parameter, the Kuramoto model can be rewritten as

$$\dot{\theta}_i = \omega_i + Kr \sin(\psi - \theta_i), \quad i = 1, \dots, N. \quad (1.41)$$

This form highlights the mean-field character of the model [23]. The oscillators now interact through the mean-field quantities r and ψ . The phase θ_i is pulled towards the

mean phase ψ . And the effective coupling strength becomes Kr , so it is modulated by the degree of phase synchronization r . This creates a positive feedback loop, wherein as the system phase synchronizes more, the coupling becomes stronger and so the system tends to phase synchronize even more. This is a very clear mechanism for spontaneous synchronization [23].

These equations always have a solution for $\theta_i = 0, \forall i$. What about others? Kuramoto considered these equations in the infinite size limit $N \rightarrow \infty$. By seeking steady-state solutions, with r constant noted that oscillators will distribute into two groups: (i) with $|\omega_i| < Kr$ which phase-lock together and (ii) with $|\omega_i| > Kr$ which keep rotating with nonuniform velocity $\dot{\theta}_i$. He then showed that a branch continuously bifurcates from $r = 0$ at $K = K_c$, a critical coupling strength, given by:

$$K_c = \frac{2}{\pi g(0)} \quad (1.42)$$

Near $K = K_c$, this branch has a square-root behavior: $r \propto \sqrt{K - K_c}$. In particular for ω_i following a Lorentzian distribution, one can show that [24, 23]

$$r = \sqrt{1 - \frac{K_c}{K}}, \quad (1.43)$$

as illustrated in Fig. 1.8C. One can verify this behavior numerically: Fig. 1.8D illustrates the results of simulations for a network of $N = 1000$ oscillators under a Gaussian distribution with zero mean and unitary standard deviation. The y -axis denotes the time-averaged behavior of $r(t)$, which oscillates in time.

Many open questions remain from the treatment just shown, such as the stability of these branches. There have been many extensions made to this model [25, 26]. In the context of multistability, some basic results come from studying an even simpler configuration, where the units are identical and coupled in a k -nearest-neighbor ring.

1.4.2 Multistability in homogeneous case: twisted states

In the case of homogeneous oscillators with $\omega_i = \omega$ coupled in a k -nearest-neighbor topology, the equations become

$$\dot{\theta}_i = \omega + \epsilon \sum_{j=i-k}^{j=i+k} \sin(\theta_j - \theta_i). \quad (1.44)$$

One can switch to a corotating frame with angular velocity ω to get rid of the ω term and appropriately rescale time to get rid of ϵ and simplify down to

$$\dot{\theta}_i = \sum_{j=i-k}^{j=i+k} \sin(\theta_j - \theta_i). \quad (1.45)$$

Note therefore that changing the coupling strength in this system only rescales time, and does not change the state space significantly! This can be written as a gradient system $\dot{\theta} = -\nabla U(\theta)$, where $U(\theta)$ is a scalar differentiable function of $\theta \in \mathbb{R}^n$ [27, 1]. As a consequence, the only attractors in this system are equilibria [27]. Therefore to find

all the attractors in the system one can first find the equilibria and then determine their linear stability. By doing this this, one finds that the equilibria obey the relation:

$$\theta_i = \omega t + \frac{2\pi q}{N} i + C \quad (1.46)$$

where $C \in \mathbb{R}$ is a constant and $q \in \mathbb{Z}$ is the twisting number. If one looks at the phase difference between two adjancent units one sees that it is constant across the ring: $\theta_{i+1} - \theta_i = \frac{2\pi q}{N}$. In particular, the completely synchronized is included here in the $q = 0$ case. Some important stability results are:

- For small values of k many twisted states can be stable. As k is increased, these twisted states start to lose stability, with higher q values starting earlier. Eventually, the completely synchronized state ($q = 0$) becomes globally stable at $k > k_c \approx 0.34N$ [27].
- If we fix k and look at estimates of the size of the basins of all stable twisted states we find that they can be parametrized by a Gaussian curve [27, 28] (Fig. 1.8E).
- Estimates of the size of the basin of attraction for $q = 0$ increase monotonically with k (Fig. 1.8F): the completely synchronized state starts to dominate the state space for denser networks [27].
- The shape of the basins is still a topic under research, but they appear to form octopus-like structures. The twisted state itself (a point) is on the head of the octopus, which a small volume around it. The majority of the volume of the basin is concentrated on the tentacles, which are structures that spread around in state space [28].

Studies have also been made for other topologies. Some important results have accumulated to show that networks with homogeneous frequencies are guaranteed to globally synchronize if the nodes are sufficiently well connected (if the networks are sufficiently dense). Taking the least connected node, with degree k_{\min} , and comparing it with the maximum possible degree of the network, $N - 1$, one can define the network's connectivity μ as the ratio $\mu = k_{\min}/(N - 1)$. Then, in networks with $\mu > \mu_c$, the only attractor is the fully synchronized state. Estimates have that $\mu \in [0.6818, 0.7889]$ [29, 30].

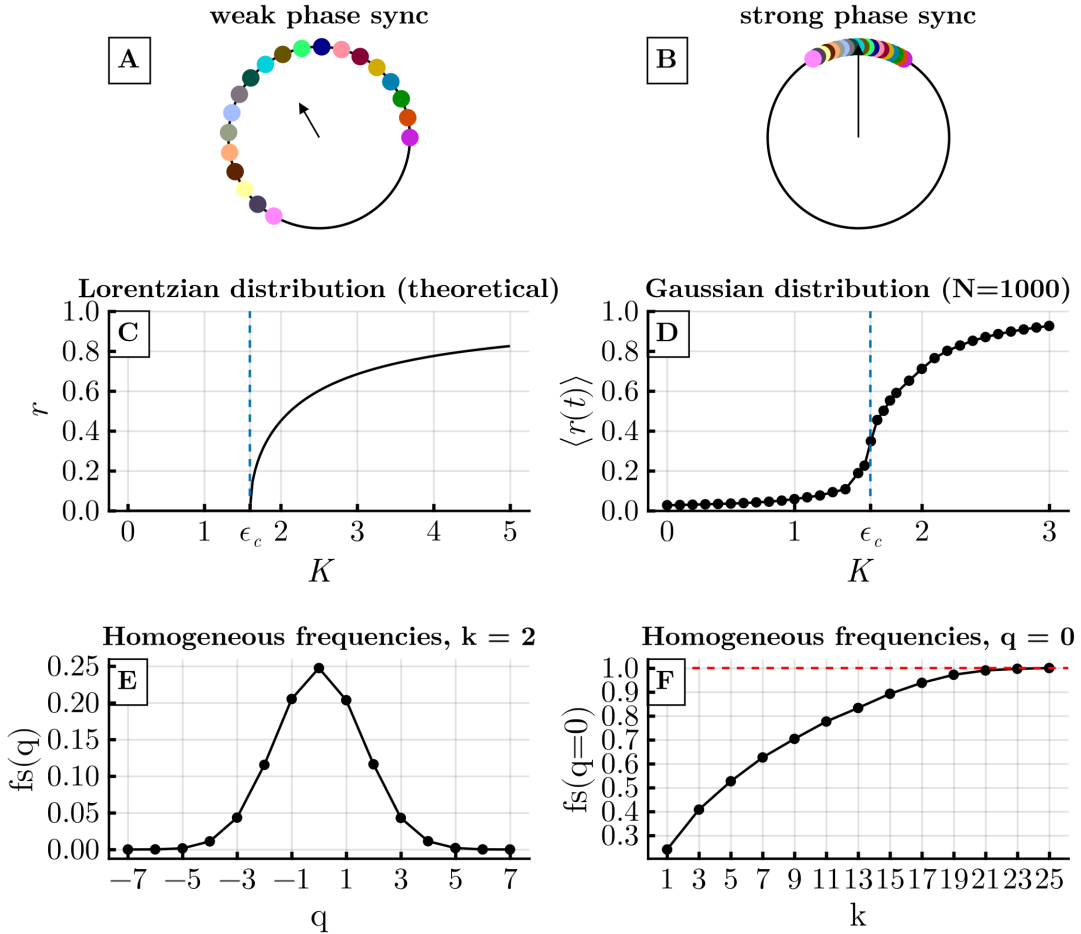


Figure 1.8: **Basics of Kuramoto oscillators.** Panels A and B respectively illustrate the concept of weak and strong phase synchronization (PS), captured by the complex order parameter Z (Eq. 1.40). The radius r denotes the degree of PS and the angle ψ denotes the centroid of the phases - respectively, they correspond to the magnitude and direction of the arrow in the figure. Panel C illustrates the behavior of the order parameter r as a function of coupling strength K (see Eq. 1.39) for a Lorentzian distribution of the frequencies (Eq. 1.43). The blue line denotes the critical coupling strength for the transition to synchronization. Panel D illustrates a similar behavior obtained from numerical simulations in a network of size $N = 1000$ under a Gaussian distribution of the natural frequencies. Only one attractor is ever observed in the simulations. Going now to homogeneous frequencies, panel E illustrates the fraction fs of randomly chosen initial conditions that converge to each q twisted state, in a network with $k = 2$ nearest neighbors. Panel F looks at this fraction for the completely synchronized state ($q = 0$) only, under different values of k . Panels E and F replicate results from [27].

Chapter 2

Small changes at single nodes can shift global network dynamics

Abstract

Understanding the sensitivity of a system's behavior with respect to parameter changes is essential for many applications. This sensitivity may be desired - for instance, in the brain, where a large repertoire of different dynamics, particularly different synchronization patterns, is crucial - or may be undesired - for instance, in power grids, where disruptions to synchronization may lead to blackouts. In this chapter¹, we show that networks of coupled phase oscillators with nonlinear interactions can acquire a very large and complicated sensitivity to changes made in either their units' parameters or in their connections. Even modifications made to a parameter of a single unit can radically alter the global dynamics of the network in an unpredictable manner. This occurs over a wide parameter region, around the network's transitions to phase synchronization. We argue that this is a widespread phenomenon that can be expected in real-world systems, extending even beyond networks of oscillators.

2.1 Introduction

Several systems of practical and theoretical importance are composed of, or can be modeled as, networks of interacting units. Examples from different research areas include power grids (networks of producers and consumers of electrical energy) [31], food webs [32], networks of electronic elements [33], coupled lasers [34], and neurons in the brain [35]. An important question is how the dynamics of single units impact the network's overall dynamics, and what happens if these units are modified. What happens to the dynamics if the units' parameters change? For instance, in ecological systems, what happens if the reproduction rate of a prey increases? In power grids, can a change in the parameters of a single generator cause a large disruption, such as a blackout? Also, what happens if the units' dynamical states are modified, e.g. by shocking the units into a different state? In the brain, how can an epileptic seizure be stopped by employing a current pulse in one particular brain region? These questions highlight the idea that a regime in which single-unit-changes can alter the whole network's behavior can be either dangerous or advantageous, and is an important topic of research which we address in this work.

In both power grids and the brain, an important phenomenon is synchronization, i.e. the coherence of frequencies or even phases of oscillations. For example, it is crucial for power grids to have their elements synchronized in the 50 – 60 Hz regime [36]. Moreover,

¹This chapter is a modified form of a published manuscript: Kalel L. Rossi, Roberto C. Budzinski, Bruno R. R. Boaretto, Lyle E. Muller, and Ulrike Feudel. *Physical Review Research* **5**, 013220 (2023).

several functional roles have been ascribed to synchronization in the brain [37, 35, 38]. For systems in which synchronization is an essential process for functioning, the question of sensitivity with respect to perturbations becomes particularly important. This has been recognized in the literature, and various types of perturbations have been considered to study the vulnerability either of the synchronized state itself or of the transition to synchronization [39, 40].

In this work, we show that systems become very sensitive to changes in parameters during transitions to synchronization, such that even changes to parameters of single units can radically alter the dynamics of the whole system. We call this phenomenon *dynamical malleability* [41], characterized by the fluctuations in network behavior caused by changes in the units' parameters or connections. Dynamical malleability can cause problems in real-world systems in two major ways: (i) the fluctuations in the dynamics can have a large magnitude, which can lead to drastic changes in the system's spatiotemporal dynamics and (ii) fluctuations are complicated and hard to predict, so that it is unclear which units or new parameter values can keep the networks in a similar synchronization state, and which others can not. Indeed, no method available in the literature to describe phase synchronization worked satisfactorily to predict the fluctuations we observe. This clearly important issue for the design and control of systems motivates our study to analyze the mechanisms that lead to these large fluctuations.

To address it concretely, we study networks of Kuramoto oscillators organized in ring lattices. They constitute a paradigmatic model for synchronization [42, 25, 26] and have been established as a model for real-world systems like the brain [43, 44, 26], Josephson junctions [45, 33], and chemical oscillators [46, 47]. The Kuramoto oscillators are phase oscillators coupled through a sine function of their phase differences. Networks with these units are well-known to have a transition from desynchronization (incoherent phases) to frequency synchronization (i.e. phase-locking, meaning constant phase differences [39]) and to phase synchronization (small phase differences) [48] as the coupling strength between units increases [26, 25].

In this work, we connect the oscillators in either of two classes of network topologies, which are of theoretical and practical importance [49]: Watts-Strogatz [21, 50, 51] and distance-dependent [52, 53]. They have very distinct properties, but in both a change in the topology from short-range to long-range connections leads to a transition to phase synchronization in the networks [54, 52]. During the transitions to phase synchronization, when the systems are only partially phase synchronized, they become dynamically malleable (i.e., sensitive to parameter changes), as illustrated in Fig. 2.1.

Furthermore, we also show that the number of attractors of the Watts-Strogatz networks increases during their transitions to phase synchronization, meaning that these systems also become especially sensitive to perturbations made to their units' states. This goes in line with recent studies for Kuramoto oscillators with identical frequencies [29, 28, 30] and for Kuramoto oscillators with inertia [14]. This increased multistability acts as a dynamical mechanism that can further increase the dynamical malleability.

Therefore, despite the wide literature and importance of synchronization, this phenomenon we describe of increased sensitivity to parameter changes, with complicated, hard-to-predict consequences to the synchronization, and which can be accompanied by multistability, has so been under-explored in the literature. Although reported sporadically in some recent works [55, 56, 57, 58], it has not been the focus, and thus has not been fully explored, until now. This becomes especially relevant when we note that the behavior is widespread, extending well beyond the Kuramoto networks studied here,

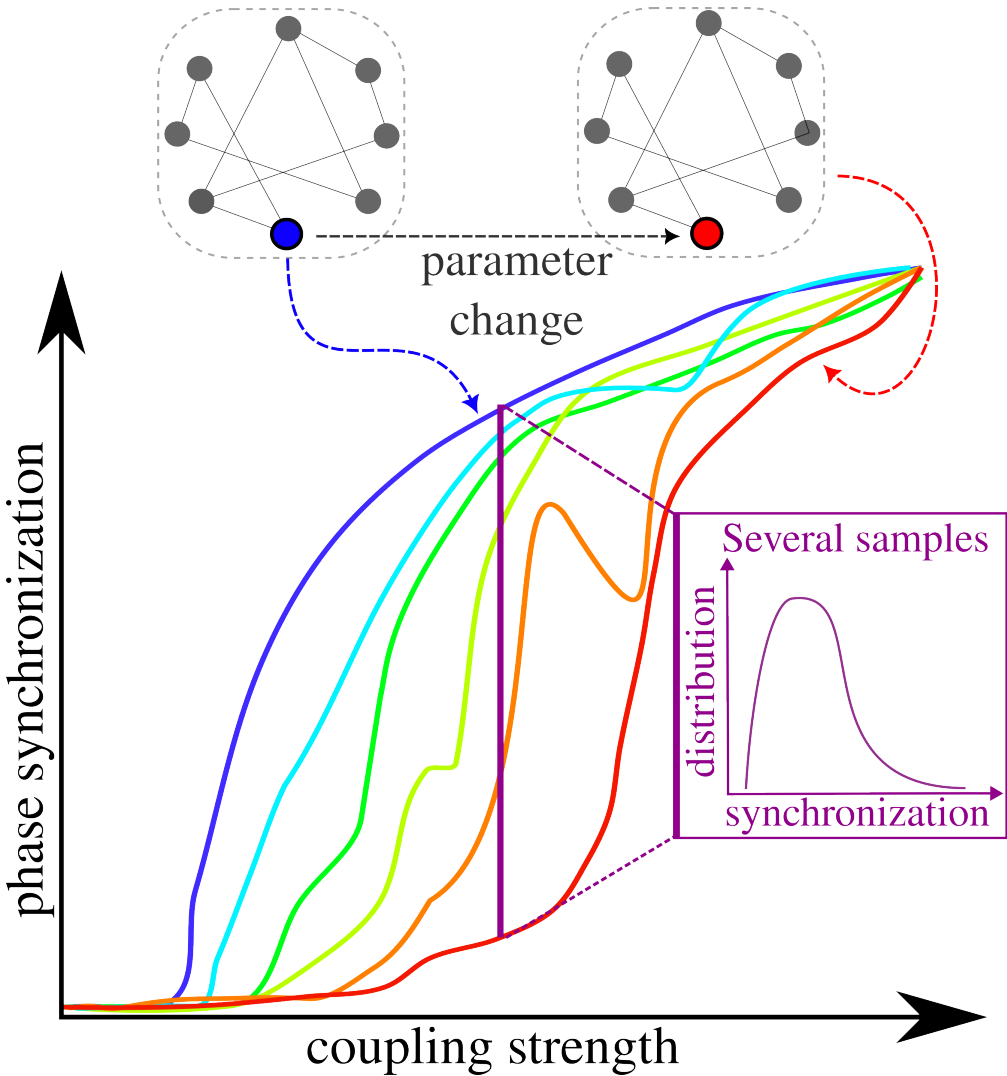


Figure 2.1: Sketch to illustrate the dynamical malleability in a typical transition to phase synchronization. Each realization of the system's parameters leads to a different transition to synchronization, i.e. a different curve in the figure. Realizations may differ from the others, for instance, in the parameter of a single unit. We see that the transitions to synchronization are different, as both the critical value of the coupling strength and the profile of the transitions differ, with the magnitude of malleability peaking during the transitions. Fixing the coupling strength, we can also look at the distribution of the degree of phase synchronization across samples (purple inset).

as supported by our observations in a variety of topologies, by similar observations in spiking [41] and bursting [58] neural networks, in cellular automata (which we exemplify in the Supplemental Material), and, importantly, by the statistical physics theory of finite-size effects on phase transitions, which we discuss later in the chapter.

We therefore hope to demonstrate the importance of dynamical malleability, and to encourage further theoretical advancements in this area, which are needed to properly describe the wide range of behaviors and to offer tools for practical applications.

2.2 Methodology

In the Kuramoto model [42, 24], each oscillator is described by a phase which evolves in time according to

$$\dot{\theta}_i = \omega_i + \epsilon \sum_{j=1}^N A_{ij} \sin(\theta_j - \theta_i), \quad (2.1)$$

where $\theta_i(t)$ is the phase of the i -th oscillator at time t , ω_i is its natural frequency, ϵ is the coupling strength, N is the number of oscillators, and A_{ij} is the (i, j) -th element of the adjacency matrix \mathbf{A} . Throughout this work, we initially draw each frequency randomly from a Gaussian distribution with mean $\mu = 0.0$ and standard deviation $\sigma = 1.0$, generating a sequence $\{\omega_i\}, i = 1, \dots, N$. Then, different realizations can (i) shuffle these frequencies, generating another sequence $\{\omega_i\}_{\text{shuffled}} = \text{shuffle}(\{\omega_i\})$; or (ii) switch the frequency of one selected unit to another value ω_{new} .

The networks in this work are coupled in a ring lattice of $N = 501$ units with periodic boundary conditions, and follow one of two classes of topology. The first class is the Watts-Strogatz (WS) [21], which interpolates between regular and random topologies with a parameter p , the rewiring probability: at one extreme ($p = 0$), the topology is a k -nearest-neighbor lattice. From it, connections are randomly chosen according to the probability p and rewired to another randomly chosen connection. In doing this, the networks have a significant decrease in the mean distance between nodes, but remain very clustered, generating small-world topologies. The other extreme ($p = 1$) is then a random topology. These networks are unweighted, so their adjacency matrix's elements are $A_{ij} = 1$ if i and j are connected, and 0 otherwise.

The second class of networks follows a distance-dependent (DD) powerlaw scheme, in which any given node receives connections with weights decaying based on the distance to it. Each element of the adjacency matrix is $A_{ij} = \frac{1}{\eta(\alpha)(d_{ij})^\alpha}$, where d_{ij} is the edge distance between oscillators i and j , defined as $d_{ij} = \min(|i - j|, N - |i - j|)$, and $\eta(\alpha)$ is a normalization term given by: $\eta(\alpha) = \sum_{j=1}^{N'} \frac{2}{j^\alpha}$, such that the temporal evolution of the phases can be written as:

$$\dot{\theta}_i = \omega_i + \frac{\epsilon}{\eta(\alpha)} \sum_{j=1}^{N'} \frac{1}{j^\alpha} [\sin(\theta_{i+j} - \theta_i) + \sin(\theta_{i-j} - \theta_i)], \quad (2.2)$$

where $N' = \frac{N-1}{2}$ denotes half the amount of units to which i is connected to (one half of the ring's length, discounting the unit i itself). The equation explores the symmetry in the network to switch the summation across the network to a summation across only half, multiplied by 2. The powerlaw decay is thus controlled by α , the locality parameter. For $\alpha = 0$, the network is globally coupled with equal weights between every node. As α increases, the weights are redistributed, so that closer units (in terms of edge-distance) have bigger weights. At the extreme of $\alpha \rightarrow \infty$, only first-neighbors are connected.

The two classes have similarities: they have topologies dominated by short-range connections at one extreme and by long-range connections at another [59, 60]. They also have differences: the first class is sparsely connected, the other densely; the first has link-disorder (different rewirings lead to different networks), the second does not.

Integration was performed using the Tsitouras 5/4 Runge-Kutta (Tsit5) method for Watts-Strogatz networks, and an adaptive order adaptive time Adams Moulton

(VCABM) method for distance-dependent networks. The integrator method was chosen for distance-dependent networks for increased simulation speed, and results were robust to different integration schemes. All methods used the DifferentialEquations.jl package [61], written in the Julia language [62]. Additional computational packages used were PyPlot [63] for plotting and DrWatson.jl [64] for code management. The code used for simulations is accessible in the repository [65], with the parameters used in the simulations. In particular, the control parameters we used (α , p and ϵ) were generated from a uniform distribution in the range of parameters showing interesting behaviors (e.g. the transitions to synchronization), then rounded to five decimal places and used in the simulations (in the case of p , the distribution was uniform in the log scale). These values are reported in all figures and text, and we emphasize that no value was chosen specifically by hand: the behaviors we show in the figures are typical of the systems and can be obtained by randomly generating other values for the parameters.

We quantify the degree of phase synchronization of the network through the standard Kuramoto order parameter [42, 24, 25], which is the circular average of the units' phases

$$r(t) = \frac{1}{N} \left| \sum_{j=1}^N \exp(i\theta_j(t)) \right|, \quad (2.3)$$

with $i = \sqrt{-1}$. The quantifier ranges from 0 to 1: if $r(t) = 1$, all the phases are the same, and the system is completely globally phase-synchronized; if $r(t) = 0$, each oscillator has a pair that is completely out-of-phase, and the system can be completely globally phase-desynchronized or in a twisted state with units having distinct but linearly spaced phases. We typically describe networks by the temporal average $R := \frac{1}{T} \sum_t r(t)$ of their phase synchronization, with T being the total simulation time excluding transients.

2.3 Results

2.3.1 Introduction to dynamical malleability

The networks we study here, described in Eq. (2.1), follow the basic phenomenology of transitions to synchronization in Kuramoto networks [42, 25]. For very small coupling strengths ϵ , the oscillators are effectively uncoupled, and the phases oscillate without any significant correlation. As this ϵ increases, the instantaneous frequencies $\dot{\theta}_i$ align first, and the units' phases become locked, but not aligned: the system becomes frequency but not phase synchronized [39].

Then, whether the phases can align or not depends on the topology [66, 54]. In a two-nearest neighbor lattice, where only four nearby units are connected (two on each side), there is a topological limitation in the spread of interactions across the network that makes the oscillators arrange themselves in shorter-range patterns (Fig. 2.2(a)) (an exception might occur if the coupling strength is extremely high, much bigger than the relevant values studied here). If the short-range connections are randomly rewired to long-range connections, following for instance the Watts-Strogatz (WS) algorithm, the shorter-range patterns give way to longer-range patterns, and the oscillators start to phase synchronize ((b) and (c)), until eventually a strong (though not complete) phase synchronization (PS) is reached (d). This occurs at different stages for each realization: for instance, panels (c) and (k) reach a high degree of PS, with the longer-range patterns, but panel (g) does not.

In Fig. 2.2, the natural frequencies $\{\omega_i\}(i = 1, \dots, N)$ were kept constant across panels (a)-(d). Changing the frequencies, keeping the initial conditions $\{\theta_i(0)\}(i = 1, \dots, N)$ fixed, leads to a different realization (also called sample), with possibly different dynamics. If the frequency of a single unit ω_i is changed to an arbitrary new value, for instance $\omega_{\text{new}} = 3$, the network's behavior can be significantly altered (panels (e)-(h)). This is especially the case for networks with intermediate rewiring probabilities p , in which this single unit frequency change can bring the network from high to very low phase synchronization (panels (c) to (g)). The instantaneous frequencies typically remain synchronized, though their values might change. For random networks, phase synchronization is always maintained, though the instantaneous frequency values may also change.

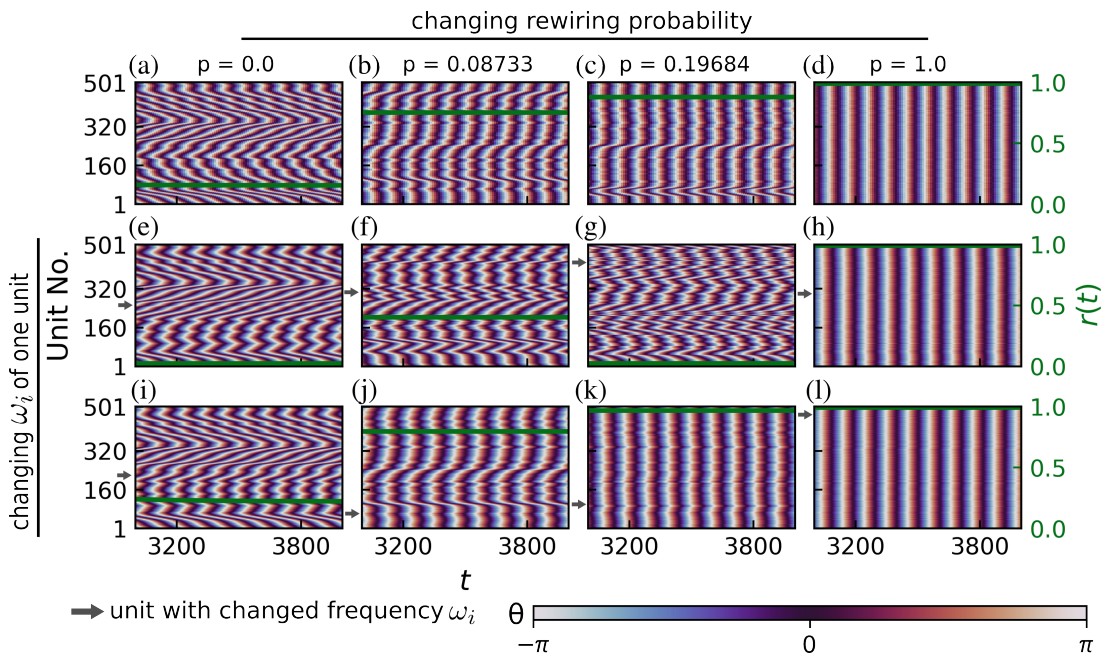


Figure 2.2: Transition to phase synchronization and the effect of a single-unit change. The figure shows the color-coded phases θ of all oscillators in the network and the degree of phase synchronization $r(t)$ (green line) across time for Watts-Strogatz networks. The coupling strength ϵ is fixed at $\epsilon = 4.51282$ and the natural frequencies ω_i in the first row are the same, generated by randomly drawing from a Gaussian distribution with zero mean and unitary standard deviation. Networks in the left column are two-nearest-neighbor lattices (rewiring probability $p = 0$); the short-range connections in these networks are then rewired in the following columns, with probability $p = 0.08733$ in the second column, $p = 0.19684$ in the third, and $p = 1.0$ in the fourth (leading to random networks). Increasing the proportion of long-range connections thus leads generally to more phase-synchronized networks. In the second and third rows, the natural frequency ω_i of a single unit i (indicated by the gray arrows) is changed to a new value $\omega_i \rightarrow \omega_{\text{new}} = 3.0$, with all other parameters being kept fixed. The units shown in the figure were those which led to the smallest (second row) or highest (third row) degree of phase synchronization R out of all $N = 501$ units in the network for each value of p . Initial conditions were the same for all simulations, and were randomly drawn between 0 and 2π .

Figure 2.2 thus illustrates that the long-term dynamics and phase synchronization

differ in each realization. The realizations, created by changing the natural frequency of one unit, are distinct dynamical systems, so it is not surprising to observe distinct long-term dynamics. It is, however, interesting to observe how large these changes in dynamics can be, and how they depend on the topology. For instance, in networks of intermediate p (second and third columns of Fig. 2.2, the phase synchronization changes drastically. In random networks ($p = 1$, fourth column), they preserve the phase synchronization but alter the instantaneous frequencies of the oscillators (seen in the figure by the number of vertical lines). We also note that the behavior we describe is typical of the systems, and the values of p and ϵ used here were generated as described in Section 2.2. Since the fluctuations in the phase patterns (reflected in the phase synchronization) are clearer and more pronounced than the instantaneous frequency patterns, we now focus on the phase synchronization of the networks.

2.3.2 Comprehensive view of dynamical malleability

To obtain a comprehensive picture we now study an ensemble of samples obtained by shuffling the frequencies ($\{\omega_i\}_{\text{original}} \rightarrow \{\omega_i\}_{\text{shuffled}} = \text{shuffle}(\{\omega_i\}_{\text{original}})$) or by changing the frequency of only a single unit to a new value ($\omega_{i,\text{original}} \rightarrow \omega_{\text{new}}$). We show in Fig. 2.3 the transitions to phase synchronization with increasing coupling strength or with switching from short-range to long-range connections. As expected from Fig. 2.2 we also find a large dynamical malleability (sometimes simply called malleability) during the transitions.

We study two classes of topology, Watts-Strogatz (WS, small-world) and distance-dependent (DD), described in Sec. 2.2. We consider ensembles as collections of networks with fixed coupling strength ϵ and topology (fixed rewiring probability p or locality parameter α) but distinct realizations of the natural frequencies $\{\omega_i\}$ [67]. Each ensemble in the figure contains 501 samples (realizations). We present the results using the mean degree of phase synchronization R for each realization, and the gap $\Delta := R_{\max} - R_{\min}$ between the most and least phase synchronized realizations in each ensemble. The gap Δ is chosen simply to illustrate the wide range of R values clearly, and we remark that very similar curves are observed by using the standard deviation over samples.

In Fig. 2.3, thicker lines represent an “original” sequence of frequencies $\{\omega\}_{\text{original}}$, from which other realizations (light lines) are created by shuffling all frequencies or changing the frequency of one unit to a new value $\omega_{\text{new}} = 3.0$. Each sample is a different dynamical system, and has a different transition to phase synchronization, which occurs at different values of ϵ , p , or α , and with a different profile (some have a small region of desynchronization while others do not, for instance).

This means that changing samples can lead to large changes in the behavior of the system, as we see throughout Fig. 2.3. First, we study the transitions induced by increasing the coupling strength ϵ for four representative types of networks (panels (a)-(d)), characterized by four specific values of rewiring probability p and locality parameter α .

In the red curves, networks are dominated by long-range connections, with $p = 1$ (random) and $\alpha = 0$ (all-to-all) and have a complete transition to phase synchronization (reaching $R \sim 1$), with the dynamical malleability (measured by Δ) increasing during the transition and returning to zero after. The all-to-all case is the finite-size version of the system originally studied by Kuramoto [24], and the critical ϵ values, when the transition occurs in each sample, are close to the $\epsilon_c = \frac{2}{g(0)\pi} = \frac{2\sqrt{2}}{\sqrt{\pi}} \approx 1.596$ predicted

in the thermodynamic (infinite network size) limit. Its finite-size scaling properties and behavior have also been studied in [68, 55]. It is worth mentioning that this parallel between random networks and all-to-all networks, which have similar phenomenology, has been described in other works. Both have the same scaling exponents, belonging to the mean-field type [59, 60].

In the green curves ($p = 0.19684$ and $\alpha = 1.538463$) some connections have been rewired in the Watts-Strogatz networks, and weights redistributed for distance-dependent networks, from long-range to effectively short-range connections. On average, phase synchronization R decreases, though still remaining high. Some samples of WS networks also start to display regions of desynchronization: after the initial transition to high R , a further increase in ϵ can desynchronize them (visible in panels (a) and (c), for ϵ roughly in [6, 7]). Therefore, the huge changes in R ($\Delta \sim 0.99$) due to changing samples can be attributed to two effects: the difference in their critical coupling strength (when the transition begins) [69], and also in their different post-transition behaviors (such as the desynchronization gaps that occur at different intervals of ϵ .)

In the purple curves ($p = 0.08733$ and $\alpha = 1.76923$), even more short-range connections become present. Phase synchronization R on average decreases, while the fluctuations Δ remain high and occur more evenly spread across samples.

Finally, for cyan curves ($p = 0$, two-nearest-neighbor chains and $\alpha = 3$, close to nearest-neighbor chains), the connections are short-range. Their phase synchronization is much smaller, and they do not reach a high degree of phase synchronization for any value ϵ we tested. These networks with short-range connections still have some degree of malleability, but not as high as the previous two cases.

Returning to frequency synchronization, we mention that for weak coupling strengths (roughly below $\epsilon \approx 3$), most of the samples in any ensemble are not frequency synchronized (see Fig. S3). Above this value, frequency synchronization becomes more common, especially for networks with more long-range connections, such that for sufficiently high coupling all samples become frequency synchronized. This is not the case for networks with mostly short-range connections ($p \lesssim 0.01$), in which some samples do not reach frequency synchronization even despite strong coupling. The presence of frequency synchronization in the short-range networks is consistent with the literature [70, 25] showing that frequency synchronization in first-nearest-neighbor chains is possible for sufficiently high ϵ in strictly finite systems. There are therefore also sample-to-sample fluctuations in the frequency synchronization of Kuramoto networks. They occur similarly to the fluctuations in phase synchronization, but are somewhat harder to visualize and have a less interesting dependence on parameters, justifying our focus on phase synchronization in this chapter.

We now move to the topology induced transitions, which occur by switching from short-range to long-range connections (varying p and α) while keeping the coupling strength ϵ fixed (Figs. (e-h)). A similar scenario occurs with a transition to phase synchronization, induced by changing either p or α . The dynamical malleability increases during the transitions, reaching significant values for both shuffled realizations and single-unit changes. The nearest-neighbor networks show some malleability, while the long-range dominated ones (random or all-to-all) show no malleability. We note here that the transition for WS occurs at $p \sim 0.1$, so we plot the figures on logarithmic scale to show the full transition to synchronization. This transition was already reported for WS networks in [54], but the authors used a linear scale for p and missed the full details of the transition that we see here, especially the sample-to-sample fluctuations; for distance-

dependent powerlaw networks, a transition in phase and frequency was reported in [52]. However, none of these references studied the sample-to-sample fluctuations.

We conclude that either shuffling or changing a single unit can significantly alter the behavior of these systems, leading to a large dynamical malleability, in some cases over a very large range of parameters. This is particularly strong for WS networks, reaching $\Delta \sim 0.99$, close to the maximum possible value of $\Delta = 1.0$. The distance-dependent networks have weaker fluctuations, though still significant, reaching up to $\Delta \sim 0.7$.

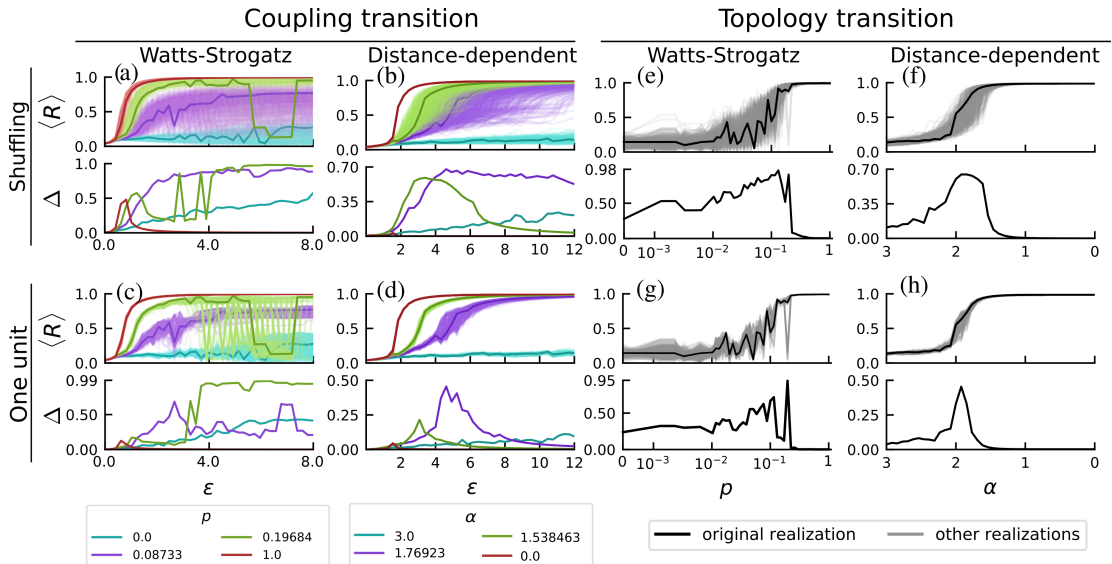


Figure 2.3: Transitions to phase synchronization and dynamical malleability. Networks under Watts-Strogatz (WS) and distance-dependent (DD) topologies reach phase synchronization through either an increase in coupling strength ϵ (given the topology has a sufficient amount of long-range connections) or by switching short-range connections to long-range. Fluctuations in the degree of phase synchronization R between samples increase during the transitions, as can be seen by the differences in the same-colored curves and by $\Delta := R_{\max} - R_{\min}$. Starting from a natural frequency sequence originally drawn from a Gaussian distribution (thicker lines), the other samples (thinner lines) can be generated by shuffling the natural frequencies or by switching the natural frequency of one unit to $\omega_{\text{new}} = 3$. For intermediate networks (purple and green curves), the increase in the fluctuations (i.e. in dynamical malleability) extends for a wide range of parameters and becomes considerably large. Each panel contains $501 = N$ realizations, with rewiring probabilities fixed for the coupling transition, with values shown in the legend, and coupling strength fixed in the topology transition at $\epsilon = 4.51282$ for WS and $\epsilon = 6.46154$ for DD. The initial conditions are the same across all realizations, and are randomly distributed from 0 to 2π . The curves of Δ are qualitatively similar with other dispersion measures, such as standard deviation, a possible difference being that the curves may be slightly shifted, as the measures can peak at slightly different values of the control parameter. We remark that the parameter values used in the simulations were generated as described in Section 2.2 and correspond to the typical behaviors in the system.

Furthermore, we note that the networks with intermediate p or α and the short-range networks have dynamical malleability even for high ϵ . This is consistent with

the known increase in the fluctuations near a phase transition [68, 71, 72] because the networks with these parameters remain close to the topology-induced transition. This is illustrated for WS networks in Fig. 2.4. It shows, in the p — ϵ parameter space, the average phase synchronization across samples \bar{R} on the first panel and the dynamical malleability measured by Δ on the second panel. Figure 2.4 provides a comprehensive view on both the coupling strength and the topology-induced transitions. The samples are realized here as shuffles, though a similar figure would be obtained by changing one unit. There is a single region of phase synchronization for sufficiently high coupling strength ϵ and rewiring probability p (panel (a)). Around the borders of this region, where the system is transitioning, the dynamical malleability is much higher (panel (b)). It then becomes clear that the intermediate networks (green and purple lines), are near the topology-induced transition (for instance, black line) for all $\epsilon \gtrsim 1$. As ϵ increases, the networks remain near this p -transition, and so their dynamical malleability does not decrease. For the regular networks, we first note that the p -axis is shown on a logarithmic scale, such that these networks, with $p = 0$, are still relatively close to the transition at $p_c \approx 0.1$, and thus they also present significant malleability.

Figure 2.4 also illustrates the existence of two qualitatively different types of transitions: one induced by increasing coupling strength (for sufficiently high p), and another induced by increasing p (for sufficiently high ϵ). The difference between both is in their starting points. Both are globally phase desynchronized, but in the former (red, green, and purple lines), the weak coupling strength regimes have mostly uncorrelated oscillators, with no discernible structures in the phases or even synchronization in the frequencies. In the latter (black line), there are shorter-range structures with frequency synchronization for most samples.

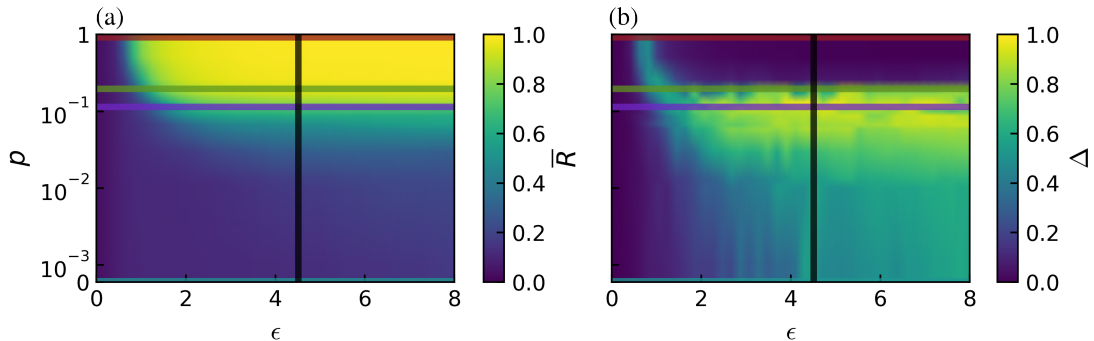


Figure 2.4: Dynamical malleability increases around the regions of transition to phase synchronization. The surface on the left shows the average degree of phase synchronization \bar{R} across the ensemble (1000 realizations of shuffled natural frequencies). The region of high phase synchronization is clearly seen for sufficiently high coupling strength ϵ and rewiring probability p . The colored lines correspond to the parameter values shown in Fig. 2.3. The right panel displays Δ , the difference between the most and least synchronized realizations for each pair (p, ϵ) , and we see that the fluctuations from sample to sample increase during the transitions to phase synchronization. The green and purple curves remain close to the region of transition for all $\epsilon \gtrsim 1$, such that their fluctuations do not decrease with an increase in ϵ . The figure uses Gouraud interpolation to ease visualization by smoothing the curves with a linear interpolation.

2.3.3 Unpredictability of dynamical malleability

For Watts-Strogatz networks, samples can be generated by resampling the topology instead of changing the natural frequencies. Since they are generated by a random rewiring process, different realizations generate different networks (there is link-disorder [60]). Therefore, different samples can also be generated by resampling the network while keeping the natural frequencies fixed. This generates a profile of dynamical malleability similar to that shown in Fig. 2.3(e), where the network was fixed and the natural frequencies were changed (see Fig. S1 for details).

Now, we wish to illustrate that no network, or natural frequency sequence, is alone responsible for leading to more, or less, synchronized states. Instead, the samples depend sensitively on both, especially in the region of large STS fluctuations. Figure 2.5(a) shows the degree of phase synchronization for different realizations of the networks and different shuffles of the natural frequencies, all for $\epsilon = 4.51282$ and $p = 0.08733$ with fixed initial conditions. To aid the visualization, red rectangles indicate the network with the largest R for each shuffle. No network synchronizes more (or less) for any sequence of natural frequencies; and no sequence of natural frequencies synchronizes more for any network. Furthermore, if the ϵ , p , or initial condition are changed, the whole profile of the figure also changes. Another way to illustrate the complicated sensitivity in the

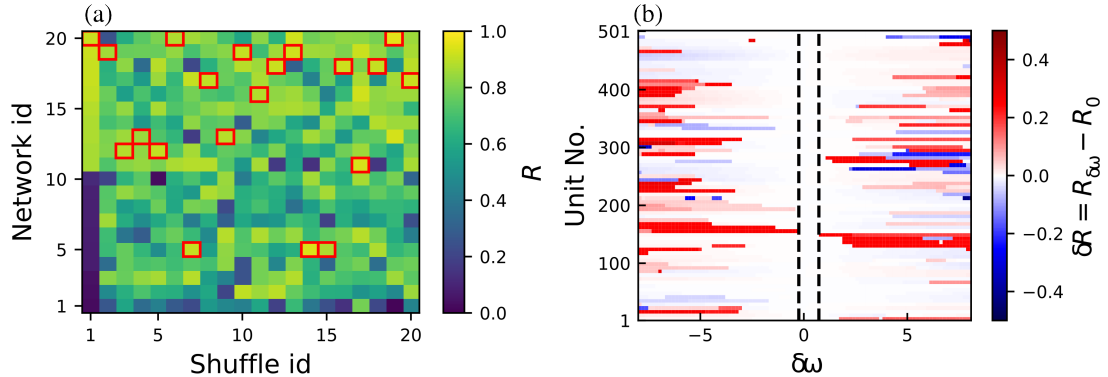


Figure 2.5: Fluctuations in dynamically malleable systems are unpredictable. Panel (a) shows the average phase synchronization R for fixed coupling strength $\epsilon = 4.51282$ and rewiring probability $p = 0.08733$ for different 20 shuffles of the natural frequencies $\{\omega_i\}$ and samples of networks generated by the Watts-Strogatz algorithm. For ease of visualization, the networks are ordered such that the highest network ids correspond to higher synchronization for Shuffle id = 1. For each shuffle, the network with the highest R is marked with a red rectangle. We thus see that no network synchronizes more for all shuffles: R is a function of both the specific frequency and topology samples. Panel (b) shows the changes δR in the phase synchronization R when the natural frequency of each unit is changed by an amount $\delta\omega$, such that $\omega_i \rightarrow \omega_i + \delta\omega$. Other parameters are fixed, in particular $p = 0.1145$ and $\epsilon = 4.51282$. There is a rough threshold (indicated by the black dashed lines), below which changing ω_i does not significantly alter R ($\delta R < 0.1$ for the figure). Furthermore, changing the frequency does not have a monotonic impact on the change in R : small alterations in ω_i , above the threshold, can have the same impact on R as bigger alterations.

region of high sample-to-sample fluctuations is by now fixing the network, and changing the frequency of a single unit by an amount $\delta\omega$. Fig. 2.5(b) illustrates the change

δR in the phase synchronization, compared to the synchronization of the "original" ($\delta\omega = 0$) frequency realization. There is a rough threshold, at $|\delta\omega| \gtrsim 0.1$, below which perturbations in one unit do not significantly affect the network's phase synchronization. Above this threshold, however, large changes occur. They are asymmetric on $\delta\omega$ and occur non-monotonically (increasing $|\delta\omega|$ does not necessarily lead to bigger changes). This complicated pattern we observe could make the design and control of these systems quite difficult in practice.

2.3.4 Ratio of short to long-range connections

As we have seen, the rewiring of connections in WS networks, or the redistribution of weights in DD networks, from short-range to long-range connections leads to a transition towards globally phase-synchronized regimes. During these transitions, the dynamical malleability peaks for some ratio of short-range to long-range connections. To quantify this ratio, we first define the short-range connections to/from a node i as all existing connections to/from other nodes j within an edge distance d (with index $j \in [i-d, i+d]$), with d being the range of short connections ($d = 2$ here). For WS networks, we calculate the average degree (number of connections) for short-range (K_s) and long-range connections (K_l). For DD networks, we define an analogous measure of topological influence, which is:

$$K_s := \frac{2}{\eta(\alpha)} \sum_{j=1}^d \frac{1}{j^\alpha} \quad (2.4)$$

$$K_l := \frac{2}{\eta(\alpha)} \sum_{j=d+1}^{N'} \frac{1}{j^\alpha}. \quad (2.5)$$

Note that due to the symmetry of the DD networks, nodes share the same value of K_s and of K_l . The ratio κ of short-range to long-range connections is then defined as:

$$\kappa := \frac{K_s - K_l}{K_s + K_l}, \quad (2.6)$$

so that $\kappa = 1$ if only short-range connections exist, and $\kappa = -1$ if only long-range connections exist, with intermediate cases in between. In WS networks, the number of connections is $K = kN$ (k being the amount of neighbors of each node), with the number of long connections approximately $K_l = pK$ and short-range approximately $K_s = (1-p)K$. Therefore, the ratio κ can be easily calculated to be approximately $\kappa = 1 - 2p$. For DD networks, the ratio κ is given as

$$\kappa = \frac{\sum_{i=1}^d i^{-\alpha} - \sum_{i=d+1}^{N'} i^{-\alpha}}{\sum_{i=1}^{N'} i^{-\alpha}}. \quad (2.7)$$

Figure 2.6 shows this ratio κ calculated for the same setup of Fig. 2.3(e) and (f), shuffling natural frequencies with fixed coupling strength and changing p or α . The dynamical malleability is measured here by standard deviation χ across the samples, instead of Δ . The former makes the figure clearer, but the same analysis also works using Δ . A remark when comparing with Fig. 2.3 is that the two measures may peak at slightly different values of p or α . For both types of networks, the malleability peaks

when there is a relatively small number of long-range connections present in a short-range-dominated network. It is more extreme for WS, as the ratios are closer to 1 than in the DD networks. This discrepancy in the ratios leading to higher malleability shows that κ is not an universal feature for any topology, but can still be important to understand their behavior.

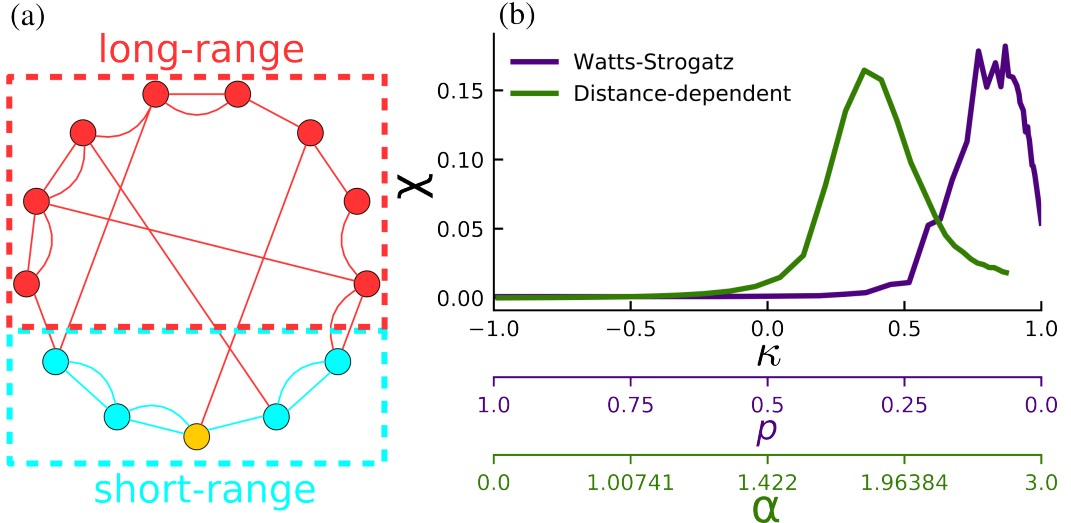


Figure 2.6: Dynamical malleability peaks within a narrow interval in the relation of short-range to long-range connections. Panel (a) illustrates the short-range (blue) and long-range (red) connections from the yellow unit for $d = 2$. Panel (b) shows the sample-to-sample fluctuations in the phase synchronization measured as the standard deviation χ of the distribution function of R against the ratio κ of short-range to long-range connections calculated for several distinct topologies p and α . The green curve corresponds to the distance-dependent networks, with $\epsilon = 6.46154$ and 501 realizations per α ; purple corresponds to Watts-Strogatz networks, $\epsilon = 4.51282$ and 1501 realizations per p . The bottom axis show the values of p and α for the respective ticks in κ (note that values of α are not equally spaced).

2.3.5 Multistability

So far, we have changed natural frequencies while keeping initial conditions fixed. Now we invert this, and shuffle initial conditions to study the system's multistability. We continue examining phase synchronization (PS) R , although we know that R is only a rough measure of multistability. Being a mean value, the same R could represent different attractors. Therefore, the number of attractors estimated based on R can only be considered as a lower bound. To remedy this, we also verified the findings by comparing several other features of the dynamics. These included the standard deviation of PS in time, the PS between each unit and its neighbors, the PS between sections of 100 units, the time-averaged instantaneous frequencies $\dot{\theta}_i$ of units, and the standard deviation, inter-quartile interval and gap between the unit's instantaneous frequencies. Realizations with unique values of all these features were considered as a distinct attractor. The number of such attractors agrees qualitatively with the dispersion we see in R , increasing during the transition.

The phase synchronization is thus shown in Fig. 2.7. Random networks ($p = 1$, red) are multistable only during their transition to phase synchronization. Intermediate networks ($p = 0.19684$, green; $p = 0.08733$, purple) have a high degree of multistability, meaning coexistence of several attractors, with very distinct degrees of phase synchronization. No shuffle of the initial conditions leads here to the same attractor, so the system has at least 501 attractors, the number of different realizations tested. The 2-nearest-neighbor lattice has significant multistability for $\epsilon \gtrsim 4$. This is consistent with the literature for 1-nearest-neighbors, in which multistability occurs after the transition to phase-locking [73].

This multistability can enhance the sensitivity of the system to parameter changes, and help to explain the large fluctuations we observe. In this case, a parameter change needs only to change the boundaries of the basins of attraction for the same initial condition to land on a completely different attractor. Attractors do not have to be necessarily drastically changed for the large dynamical malleability to be observed. However, multistability is not in principle required for STS fluctuations; in fact, the distance-dependent networks appear to be monostable (not shown), though they are malleable.

2.3.6 Distributions of samples

As we have seen, shuffling initial conditions can also generate realizations with widely different dynamics, similarly to shuffling natural frequencies. But the two methods to create an ensemble of samples have different effects, and can generate samples with distinct distributions. As shown in Fig. 2.10 for Watts-Strogatz networks, shuffling frequencies leads usually to a broader, and smoother, distribution of R . This increased broadness shows that new attractors are indeed created by shuffling the frequencies, so that multistability itself cannot account for the dynamical malleability we discussed previously. Furthermore, the transitions to phase synchronization occur through an increase in the distribution's average. The accompanying increase in the width of the distribution shows an increase in dynamical malleability, which goes to zero only for long-range networks ($p = 1$).

Specifically, the distributions for the two-nearest-neighbor lattice ($p = 0$, panels (a)-(e)) are quite different: shuffling frequencies leads to a smooth distribution, whose average shifts to the right as ϵ is increased; for shuffling initial conditions there is also a slight increase in the distribution's average as ϵ is increased, but the distribution itself is dominated by several peaks. For intermediate networks ($p = 0.08733$ and $p = 0.19684$, panels (f)-(o)), the skewness of the distribution becomes negative, and shuffling initial conditions has a smoother behavior, more similar to shuffling frequencies. Interestingly, the distribution can be bi-modal, with the two modes being separated on either extreme of R (panels (n) and (o)). For $p = 1$ (random network), the two first coupling strengths (panels (p)-(q)) occur during the narrow interval of significant malleability, during the transition to phase synchronization. Soon after $\epsilon > \epsilon_c \approx 1.6$, the distribution becomes extremely narrow.

It is worth mentioning that very similar distributions are obtained if, instead of shuffling the frequencies or initial conditions, we re-sample them from the distribution (i.e. change the seed in the random number generator). Interestingly, the distributions are not Gaussian, which is inconsistent with the assumptions made in other works [68, 60]. In these works, the authors argue that the fluctuations must be normally distributed for sufficiently large networks and many samples due to the central limit theorem. This

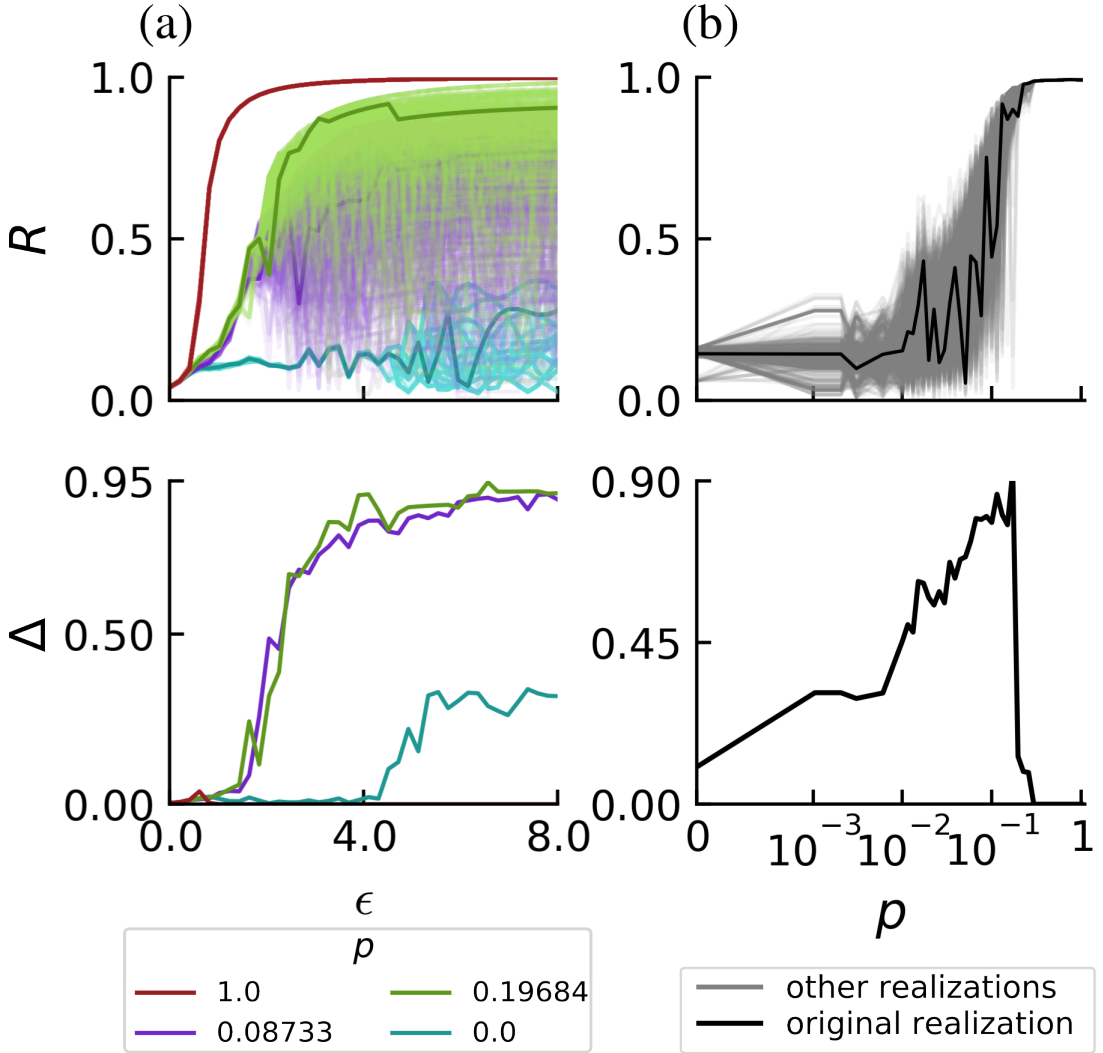


Figure 2.7: Multistability in WS networks. Phase synchronization and its dispersion for 501 different shuffles (thinner lines) of the initial conditions, taken from the original initial conditions (thicker lines) used throughout the rest of this work. All other parameters are fixed, including the natural frequencies as the original frequency distribution. The coupling strength ϵ (left panel) and rewiring probabilities p (right panel) are the same ones used for WS networks in Fig. 2.3. The multistable behavior is thus very similar to what we observed before by changing the frequencies (Fig. 2.3(a) and (e)), and so shuffling the initial conditions for this network also leads to large fluctuations in the phase synchronization.

inconsistency is likely generated by the finite size of the networks studied here. Even in all-to-all networks, in which there is no topological disorder, the distributions are not Gaussian for $N = 501$. Results (not shown) indicate that the distributions approach Gaussian distributions as N is increased to 5000.

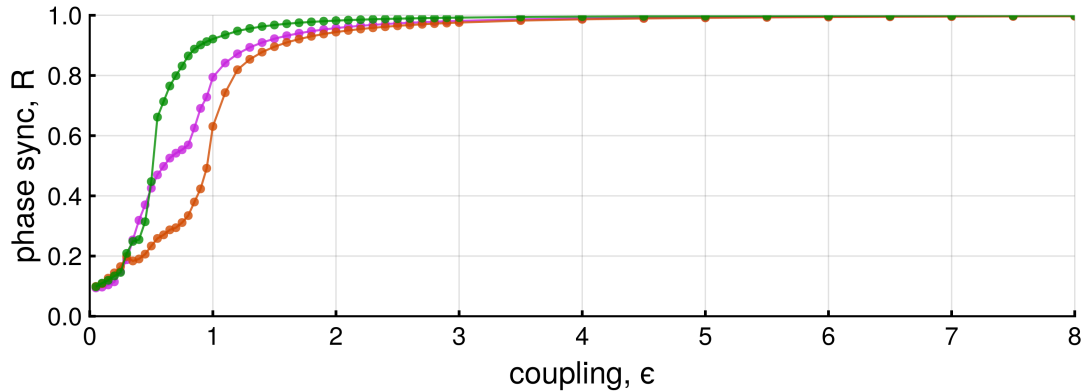


Figure 2.8: Multistability in WS networks.

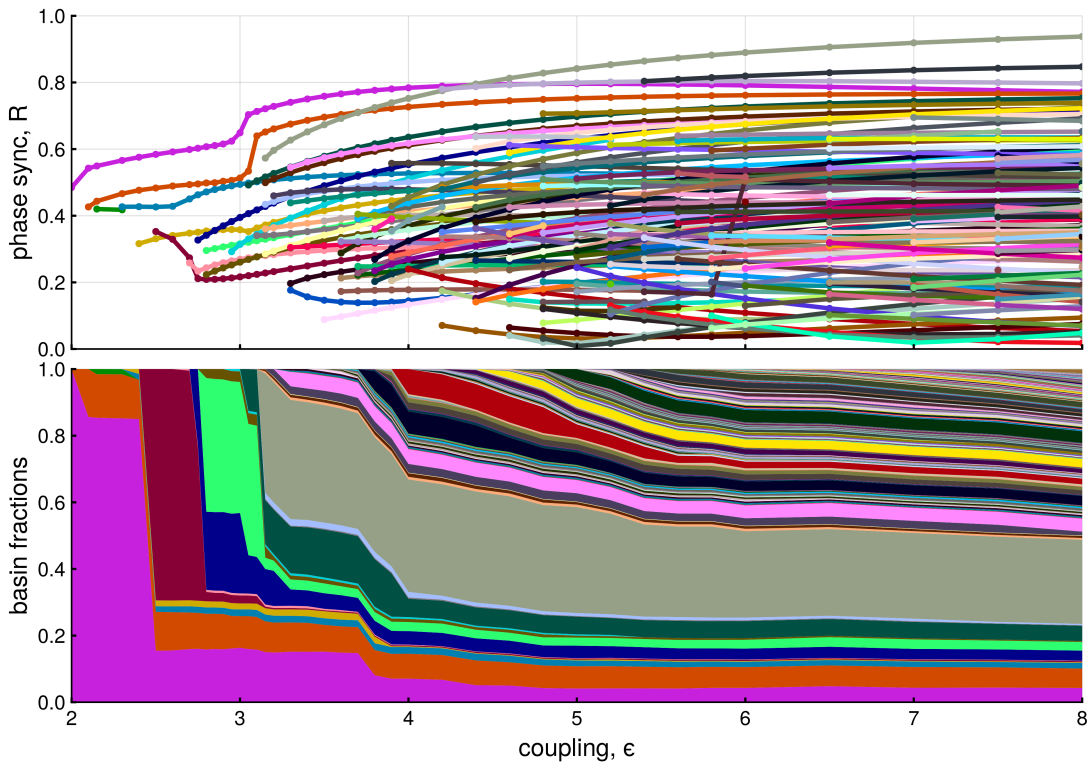


Figure 2.9: Multistability in WS networks.

2.4 Discussions and conclusions

Summary

In this work, we have studied the sensitivity of networks to changes in their units' parameters or connections, which we call their dynamical malleability, and showed that, near transitions to phase synchronization, this behavior acquires (i) a large magnitude,

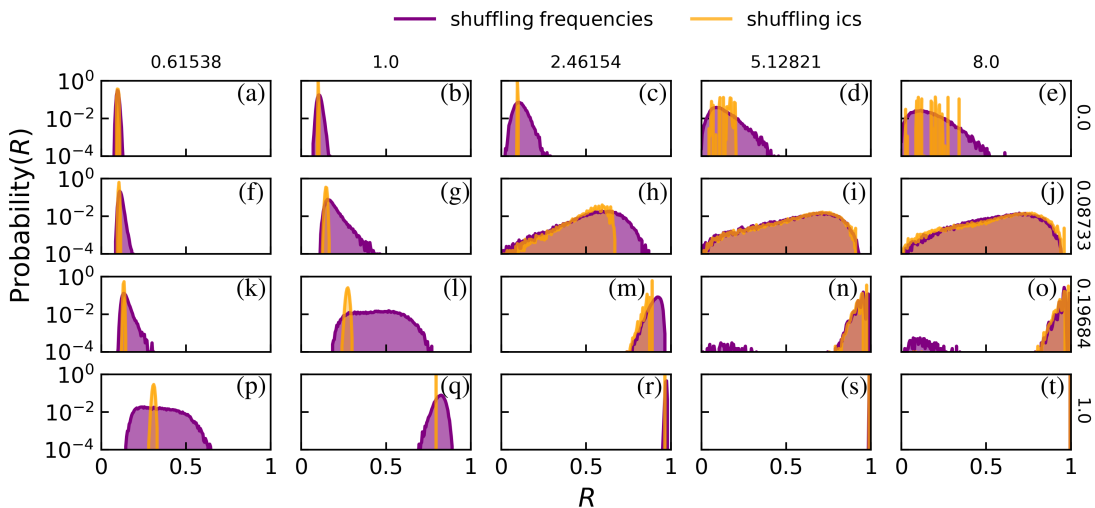


Figure 2.10: Distributions of R due to shuffling frequencies or initial conditions. Each panel contains the distribution of the mean degree of phase synchronization R across 20000 shuffles of natural frequencies (in purple) or initial conditions (orange) for Watts-Strogatz networks. The rewiring probabilities p are indicated on the right of each row, and are the same as used in Fig. 2.3(a); the coupling strengths ϵ are indicated on the top of each column. Bin size is 0.005, and the probability for each bin is calculated as the occupation of the bin divided by the total occupation across all bins, and is shown in logarithmic scale.

as changes to single units can radically alter the spatiotemporal dynamics, and (ii) a complicated sensitivity, as no analytical method we have tried was able to satisfactorily describe the changes to the dynamics. Parts of this behavior have been observed in isolation previously [41, 56, 54, 55, 57, 58] but this is, to the best of our knowledge, the first work to focus specifically on it and show its full phenomenology.

To study this concretely, we have chosen ring networks of Kuramoto phase oscillators and connected the units in two distinct classes of topology, Watts-Strogatz (WS) and distance-dependent (DD). We have either changed the frequency of a single unit or changed the frequencies of all units by shuffling (i.e., redistributing) the values of the frequencies across units. The first has allowed us to verify the impact of relatively small changes, which are still not small enough to be described in the linear regime; the latter allowed us to verify the impact of redistributing the values in the network while keeping the distribution of parameters exactly the same, which is helpful for identifying mechanisms for the fluctuations.

Mechanisms for dynamical malleability

The two classes of topology we used have different characteristics (see Sec. 2.2) but are similar in that they lead to networks that have two distinct types of transition to phase synchronization: one induced by increasing the coupling strength and another by increasing the dominance of long-range connections. They also have differences, mostly notably that (i) the WS networks acquire a large number of attractors during their transitions to phase synchronization (i.e. become highly multistable), while the DD

networks remain with one main attractor (and possible other attractors that would have very small basins of attraction), and that (ii) the WS networks have a larger magnitude of dynamical malleability. We believe that this larger magnitude is caused by two effects: the increased number of attractors and the topology's link-disorder.

Firstly, we remark that the dynamical malleability is manifested in the networks' transitions to phase synchronization in two distinct ways. The first is through diverse onsets of the transition, as different realizations start their transitions at different values of the control parameter. This is the well-known blurriness of phase transitions described in studies of finite-size effects [71, 74]. This effect is clearly present in both networks (see, e.g., Fig. 2.3(a) and (b)). The second manifestation of malleability is in the post-transition fluctuations, i.e., in the sudden changes of synchronization that occur after the network has seemingly transitioned to synchronization (see, e.g. Figs. 2.3(a) and (c)). This effect is present here mostly in the WS networks, but is also known in other systems of finite size (see, e.g. Figs. S5(b) and (d) for the case of cellular automata). It is caused at least partly by the system's multistability, as increasing the parameter can change the shape of the attractors' basins of attraction, making the same initial condition suddenly go to another attractor. So the WS networks, which have a much larger number of attractors, exhibit this additional effect that increases their malleability, while the DD networks do not.

We further remark that multistability could have an even more pronounced impact on malleability if the basins of attraction were complexly interwoven. Then, even very small changes could lead to significant fluctuations. But this does not appear to be the case in any of the networks we studied, all of which seem to have smooth basin boundaries (Fig. S4) - it is thus noteworthy that the already high dynamical malleability we have described can occur even with smooth basin boundaries. It can even occur in the absence of multistability, as seen in the DD networks.

The second mechanism for the increased malleability in WS networks is their link-disorder [60]: different realizations lead to different topologies for a same parameter, and we observe a very similar phenomenology by comparing different realizations of these topologies (Fig. S1). This is a source of disorder, and thus, of fluctuations, that is not present in the DD networks.

Mechanisms for the fluctuations

As we have mentioned, the fluctuations in the malleable networks are also hard to predict. The behavior of the systems is clearly a complicated function that involves the coupling strength, topology, natural frequencies, and initial conditions all together. For instance, we have not found a sequence of frequencies, or a specific network realization, that always leads to more (or less) synchronized networks (Fig. 2.5(a)). Even for fixed frequencies and topology, the most phase synchronized realization changes depend on the initial condition or the coupling strength. Changes in the natural frequency of single units also lead to non-monotonic changes in the network's phase synchronization: the change in frequency can either increase or decrease the synchronization level, depending on the chosen unit, coupling strength, and topology (Fig. 2.5(b)).

As a consequence, we are unable to identify a specific unit, or magnitude of perturbation, that is always responsible for the greatest disruption. That is, no available theory in the literature that we have tried revealed a mechanism for the fluctuations capable of predicting them. This is a surprising result, considering the quality of the available

theories, the amount of research and important advancements in the description of networks similar to the ones studied here [55, 75, 76, 77]. We believe that this is mainly caused by the networks' multistability, which cannot be handled by some theories, and by the wide range of synchronization patterns.

The first theory we tried is the synchrony alignment function, which depends on the topology and natural frequencies and was shown analytically to be related to the degree of phase synchronization in the limit of strong synchrony [75]. It does not work satisfactorily for any dynamically malleable network that we tested. One reason for this is the weak phase synchronization in some realizations, which breaks the assumption of the method. Another, even stronger, reason is that our networks are multistable, such that the relation between the synchrony alignment function and the degree of phase synchronization given by the method cannot be satisfied for all attractors of the system. Indeed, it only worked perfectly in the strongly phase synchronized regime, which is also monostable.

The second theory we tried is due to Peter and Pikovsky [55], who showed in all-to-all networks that different realizations of the natural frequencies synchronize differently depending on the kurtosis of the distribution. This mechanism cannot even be expected to work for the shuffling scenarios we study since they conserve the frequency distributions and thus the kurtosis as well, but we have verified that it also does not work when the units' frequencies are changed. An additional reason why this does not seem to apply in our systems may be in the topologies, which are not all-to-all.

Thirdly, we have tested other measures that have been observed in the literature to correlate to phase synchronization, and they do not work in the malleable networks. These are: (i) the proportion p_- of links connecting nodes with natural frequencies of different signs [76]; (ii) the correlation c_ω between the oscillators' natural frequencies, taking into account the connectivity of the network [76, 77]; (iii) the correlation between natural frequencies and the node's number of connections [75]; and (iv) the correlation between the average frequency between neighbors of a node and the node's own frequency [78, 75]. These results also cannot be expected to work in multistable networks, and indeed did not work in our networks.

Relation to statistical physics and scaling

As noted previously, there is a relation between our dynamical study here and studies on the statistical physics of networks. The transitions to phase synchronization that we see correspond to non-equilibrium phase transitions [24, 55], such that we can connect the dynamical malleability we analyze with the well-known sample-to-sample (STS) fluctuations in statistical physics. These are usually described in finite systems, in which different samples have different statistical properties that lead to distinct phase transitions - the transitions are usually said to be shifted between samples [79, 80, 68], which is one of the mechanisms we described for the malleability. As seen in these studies, the size N of the system (i.e. the number of nodes) influences the magnitude of the dynamical malleability as well as the interval of parameters in which it occurs. The networks we have presented in the results have $N = 501$ oscillators, and scaling analysis (Fig. S2) reveals that the intervals of high malleability decrease with the size N , as expected from other studies. For instance, authors in [68] describe the range of ϵ for high malleability as scaling with $N^{-2/5}$ for all-to-all networks.

For the WS networks, malleability is still significant for even up $N = 5000$ oscillators.

Moreover, the maximum magnitude of the fluctuations does not decrease significantly, and networks with $N = 5000$ can still reach $\Delta = 0.9$. This suggests that the malleability gets restricted to a smaller region in parameter space, but might not decrease significantly in magnitude for bigger networks. In the limit of infinite-size networks, it would get restricted to a single line, defining the two types of transitions to phase synchronization, and remain non-zero there. This is consistent with a study in all-to-all networks of Kuramoto oscillators, where this behavior was observed [69]. In fact, this behavior is well-known for phase transitions with quenched disorder (heterogeneous parameters), when systems are said to be non-self-averaging [81]. In any case, networks of $N = 5000$ units can be regarded as rather large in several real-world applications [55], so the STS fluctuations we describe here occur for a significant range of system sizes.

Generality of the behavior

Additionally, we show that the increase in dynamical malleability is widespread in the parameter space of the systems. Looking at this space, spanned by coupling strength and the parameter controlling the topology, the dynamical malleability remains high over a wide parameter range around the two types of transitions to phase synchronization. In particular, networks with an intermediate amount of long-range connections are highly malleable for any coupling strength ϵ we tested (e.g. green and purple lines in Fig. 2.3). This is because the topology is fixed, so the networks remain close to the topology-induced-transition even though they are far from the coupling-strength-induced-transition.

We also remark that the phenomenology we describe also occurs for wide ranges of topology and coupling strength values, for distinct frequency distributions, such as Cauchy-Lorenz (not shown), and for other dynamical models. For instance, previous works on spiking [41] and bursting [58] neural networks have revealed a very similar phenomenology. We also show similar behavior for cellular automata (see Fig. S5). We have observed (not shown) similar behavior in small-world networks generated by adding long-range connections and keeping the short-range ones [82]. Other works have also observed dynamical malleability in Kuramoto oscillators coupled under both human-connectome structural networks and hierarchical-modular networks [83, 84]. Additionally, of course, the theory of phase transitions and, consequently, of sample-to-sample fluctuations is known to apply for a variety of distinct systems.

Practical importance of malleability

The discussions lead to an interesting question: is dynamical malleability good or bad? On the one hand, large fluctuations can be undesired. For instance, a large fluctuation could take power grids from a phase synchronized regime to a desynchronized one, and lead to blackouts. On the other hand, fluctuations can be desired due to the increased flexibility in the systems. They could be a useful mechanism for adaptation, learning or memory formation in neural circuits. More specifically, an important property of the brain is that it can separately process information from different types of input in segregated areas, and then integrate them all into a unified representation [85, 86, 87]. For this reason, Tononi and colleagues conjectured that the brain needs to have an optimal balance between segregation and integration of areas [85]. In this optimal balance, the synchronization between different brain regions needs to fluctuate from low synchronization to high synchronization [88]. Therefore, having a large dynamical

malleability can be an advantageous feature, allowing for this high variability to be achieved through small changes in the neurons, e.g. their firing rate, or their connections. There is also interesting evidence for this in [89], which reported that high-frequency firing of neurons can drive changes in the global brain state.

Future research and conclusions

An interesting line of research opened here is to understand ways to quench or to explore the fluctuations between realizations, using the framework we establish here, for practical applications. Another interesting line of research is to consider the effects of noise or time-dependent forcing on malleable systems: since they have a wider range of dynamical states available by changing parameters, a time-dependent change in the parameters, induced by the noise or forcing, can lead to transitions between several different states. The complicated and sensitive dependence on the parameters would mean that even small amplitude changes could lead to drastic fluctuations. For the Watts-Strogatz networks, multistability can complicate the dependence on external inputs, and make the effects dependent on the timing of perturbations, as different states, all of which coexist, can react differently to the parameter changes. Understanding these behaviors is important, for instance, in the context of neural systems, where external influences are common and where temporal fluctuations are essential.

Future research is also needed to fully describe the mechanism for the fluctuations between realizations. An interesting possibility could be to extend the synchrony alignment function [75] to weakly synchronized regimes or to multistable systems. Another promising approach would also be to apply the formalism introduced in [90, 91]. A third possibility would also be to use the model reduction method by [92]. These would be important theoretical contributions for the understanding of phase synchronization in oscillator networks and for the role of each unit in a network.

To summarize, the increased magnitude and complexity of dynamical malleability shown here is a general phenomenon in finite-size systems that can be expected to occur in real-world systems.

Acknowledgments

We would like to thank Jan Freund and Arkady Pikovsky for helpful discussions. K.L.R. was supported by the German Academic Exchange Service (DAAD). R.C.B. and L.E.M. acknowledge the support by BrainsCAN at Western University through the Canada First Research Excellence Fund (CFREF), the NSF through a NeuroNex award (#2015276), SPIRITS 2020 of Kyoto University, Compute Ontario (computeontario.ca), Compute Canada (compute canada.ca), and the Western Academy for Advanced Research. R.C.B gratefully acknowledges the Western Institute for Neuroscience Clinical Research Post-doctoral Fellowship. B. R. R. B. acknowledges the financial support of the São Paulo Research Foundation (FAPESP, Brazil) Grants Nos. 2018/03211-6 and 2021/09839-0. The simulations were performed at the HPC Cluster CARL, located at the University of Oldenburg (Germany) and funded by the DFG through its Major Research Instrumentation Program (INST 184/157-1 FUGG) and the Ministry of Science and Culture (MWK) of the Lower Saxony State, Germany.

Chapter 3

Conclusions

Science is typically reductionist [93]. We break a hard problem into smaller parts that are easier to understand separately. We have achieved tremendous success with this effort, but we have not solved everything; indeed, we have found out that putting everything back together can be quite complicated: the interactions between the parts can generate complex behavior that is not present in any one of the parts alone. The field of complex systems arose from the need to understand this *emergent phenomena* - to (re)construct the full system's behavior from knowledge of its parts. In the case of networked systems, studied in this thesis, the challenge can be phrased as the need to understand how the whole system's behavior arises from the coupling between the units. A major challenge still today is to develop tools that allows us to characterize and understand complicated emergent behavior.

One such complicated behavior in networks is the coexistence of multiple stable solutions to the same equations with the same parameters - *multistability*! How do these solutions come about, where they are situated and how they are separated in state space - these are all questions under active research [94, 10, 28].

Some of these stable solutions may correspond to synchronized regimes, which brings into light another important phenomenon: *synchronization*. Here again the field of complex systems has to contend with another problem: how individually distinct units can cooperate together and start to operate in unison, in a beautiful example of an emergent phenomenon. The study of synchronization - both frequency and phase synchronization - also has important practical motivations, for instance in the study of power grids. In power grids, and other complex networks, understanding the robustness of solutions, in particular of synchronized solutions has been an object of active research.

Combining these two research areas, Chapter 2 investigated the robustness of solutions in a complex network of Kuramoto oscillators, a paradigmatic model for studies on synchronization phenomena and complex networks in general. The idea was to investigate how the network behaves - how the solutions change - when we alter the parameter of a single unit in the network. We found that the *dynamical malleability* of the network depends on how strongly coupled the units are, and the topology of the connections. Roughly, we showed that for very weak coupling strength the individual tendencies of the oscillators win and most of them oscillate incoherently. For sufficiently strong coupling, most of the oscillators become phase locked - they oscillate at the same frequency. This is the same behavior as in all-to-all networks (see Sec.1.4). The spatial pattern of the phases, which we can measure via the degree of phase synchronization, was then determined by the topology. For several of the coexisting attractors, including the most phase synchronized attractor, the following tendency was observed: networks dominated by short-range connections tend to have attractors with short-range patterns (phase desynchronized), while networks dominated by long-range connections tend to have attractors with long-range patterns (phase synchronized). In parameter space, phase synchronization in these networks lives in the region of sufficiently high coupling strength and number of long-range connections. Changing the parameters toward this region therefore makes the system undergo a transition to phase synchronization. We showed that precisely during this transition their dynamical malleability increases con-

siderably. To the point that changing a single unit radically alters the pattern of phases in the network, potentially changing it from phase synchronized to phase desynchronized.

The mechanism for this dynamical malleability is two-fold. First, it is related to *increased sample-to-sample fluctuations* near a phase transition [68, 80]. This mechanism does not require multistability. In fact, suppose the systems have a single attractor, like the randomly connected networks. Each change to a parameter of a unit leads to a different dynamical system, which may have a different attractor. In particular, the transition to phase synchronization of this attractor may occur at different coupling strength values, earlier or later compared to the system before the change. If we enact this change but keep the coupling strength fixed, we switch to an attractor that has a smaller or larger value of phase synchronization - this is the fluctuation from one sample to another. If the systems have multiple attractors, this effect is still there, but there is the added possibility of switching to other attractors, which might be even more different. The *multistability* increases the possible fluctuations that may occur. This explains our observation that for Watts-Strogatz networks the malleability and multistability seem to go hand in hand. It also explains why these networks have a considerably larger malleability than the distance-dependent networks, which do not seem to be multistable.

An important concept in the area of complex systems is that of global stability, typically taken to mean the relative size of the basin of attraction of each attractor. In this view, attractors whose basins occupy larger regions of state space are more globally stable [95]. The rough idea is that trajectories on attractors with bigger basins of attraction are more likely to require bigger perturbations in order to be kicked across the basin boundary and into another attractor. This is not necessarily the case, however, since the situation depends on the geometry of the basin of attraction [96], but it highlights the importance of studying perturbations applied to the state of a system. In general, more attractors means they are sharing state space more and therefore the global stability is smaller, meaning the system is less robust (or less resilient, depending on terminology [96]). In this work we show that multistability affects the robustness of the system in another way: by affecting its malleability. So not only is it dangerous to kick the state of the system, it is also dangerous to change its parameters - even the parameter of one single unit!

Another important observation was the study of how malleability, and multistability, depend on the topology of the system. Topologies that put the systems in the vicinity of a transition to phase synchronization, which were in the small-world range, made it very malleable. An important question that is left for future work is why these specific topologies lead to a higher number of attractors - which properties do they possess that lead to the emergence of the attractors, compared to, say, the random topologies, which do not induce multistability? The distance-dependent networks also do not seem to be multistable, a factor that would also be interesting to investigate.

A related question is about the generality of these results. Malleability due to sample-to-sample fluctuations is very common, being extensively described in statistical physics literature [79]. We also described it initially in a network of spiking neurons [41], and observed it in the Kuramoto model under different topologies of distributions of the natural frequency, and under other models, such as a simple model of excitable cells. We believe that the multistability results will also generalize somehow - supported by the available evidence from other works - but this is also object of future research. Understanding better the mechanisms generating the multistability will also help answer

this.

In a similar vein, we also investigated how multistability emerges when excitable neurons are coupled diffusively. Excitability in the individual units here occurs due to the presence of a saddle and an unstable equilibrium in state space, which force part of the trajectories to go around on a long excursion before eventually converging to the stable equilibrium. These region where trajectories go through is called the *excitability region*. We showed that the coupling can trap trajectories in this excitability region by repeatedly reinjecting them there. This mechanism underlies all the emergent attractors we observed, even though they arise due to different bifurcations: saddle-node of limit cycles and homoclinic. For two units, it can create three coexisting periodic attractors, and can also create a quasiperiodic attractor. For more units, it can create a larger number of attractors, including potentially a chaotic attractor. Based on the trapping mechanism and preliminary results, we conjecture that the topology of the networks plays a key role in dictating which attractors emerge, and how many. This could be very similar to Kuramoto networks, and a more in-depth comparison is definitely warranted. It would be very interesting in the future to explore how exactly the size and topology of the networks control the emerging attractors.

In this initial work we decided to focus mainly on the pure dynamics of the system, so we showed most of the results in the case where the coupling is applied to both the x and y directions of the system. In some models, such as ecological models - where the diffusive term would model a migration of species - this might be very sound. For the neuronal case, however, only the x -coupling is biophysically sound. Motivated by this fact, we also investigated how the attractors change when the coupling is applied to only one variable. Interestingly, the mechanism is still present, but the two main types of attractors we observed split up when the coupling is split. The exclusive x -coupling leads to the attractor with two units trapped in the excitability region (LA-LA); the exclusive y -coupling leads to the one with only one unit in the excitability region (LA-SA or SA-LA). We confirmed this with a bifurcation analysis and also qualitatively explained it based on the geometry of the attractors and the trapping mechanism. This is important in terms of potential applications. First, it means that adding a gap junction between two otherwise silent neurons could make them bistable, with the possibility of periodic or even quasiperiodic spiking. In fact, there is some evidence that this seems to occur in neurons coupled under gap junctions in the motor cortex of fruit flies [97]. It is also interesting in the ecological direction, if we consider that only some species in an ecological niche might be migrating between patches.

Furthermore, we focused for simplicity on the excitable case, where the trapping mechanism creating the attractors is more easily seen. But attractors still emerge similarly in a bistable regime, where the stable equilibrium coexists with a stable limit cycle. We can achieve this by changing the input current I of the model. A difference in this case is that the uncoupled neuron already has an oscillating attractor. Therefore, when they are diffusively coupled they can also synchronize together in this oscillating attractor. This system thus has the possibility of achieving full synchronization on a periodic attractor. In this case, one could reframe the study in terms of the stability, global and linear, of the synchronized state, and how the coupling might create new attractors and thus reduce the relative size of the basin of the synchronized attractor.

We initially arrived at this problem when trying to understand the synchronization behavior of a network of bursting neurons [98]. The degree of phase synchronization in that system changes nonmonotonically as a function of the coupling strength: increas-

ing the coupling initially increases the phase synchronization, then actually decreases it in a certain region, before increasing it again for very strong coupling. This is also reminiscent of a behavior observed in networks with chaotic saddles in Ref. [99]. We also studied a network of bursting neurons following another model, and found that a chaotic saddle was important there but also a slow region of system's limit cycle was related to the multistability that emerged. From the work on excitable neurons, we understand that slowness can help generate attractors, at least for the reinjection mechanism we observed. It would be interesting in the future to go back and finish the initial studies.

When working on a project, I believe it is not an uncommon feeling to find an interesting paper, try to replicate its results and not quite manage. Then, to look at the source code that the authors hopefully provided, and to be underwhelmed. While working on a paper, it is often the case that people might want spend as little time as possible implementing the algorithms they need, leading usually to confusing code, which might not be as efficient as it could, and not as well-tested - and thus, more susceptible to errors. One solution to this is to create a unified library that implements efficient code, tests and documents it. And to make it open-source, to share it with the whole community. Then, anyone can scrutinize the code, find improvements and test it further. Also, more importantly, everyone can use it. This saves implementation time, potentially run times due to improved code efficiency, and also re-implementation time for poor students aiming to replicate papers. This is the philosophy of the dynamical systems library [100], started by Dr. George Datseris, written in the Julia programming language. With this idea in mind, we also collaborated to implement algorithms related to finding attractors and their basins. In particular, I worked on the algorithm used in the two multistability works in this thesis. It is a brute-force algorithm that integrates trajectories, converts them into vectors of features, and selects attractors as unique groups of features [14, 15, 12]. Together with Prof. Alexander Wagemakers, we also implemented an algorithm that applies attractor-finding algorithms across a parameter range, in a continuation manner. The result of this work was the *Attractors.jl* package, also co-developed by more collaborators, and a publication describing this novel algorithm and improvements to previous literature [12].

So far on the study of dynamical systems we have mostly focused on attractors. The motivation for this is that attractors represent a system's long-term dynamics: after some *transient* time, trajectories converge to attractors. There is, however, a key assumption here: that the period of time during which we observe the system T_{obs} is longer than the convergence time T_{conv} to the attractor. It is a matter of time-scales: of the observation versus the relaxation to the attractor. Whether this can be guaranteed or not depends on the application. In power grids, for instance, one is generally interested in the long-term dynamics of the system. In the brain, however, changes may be occurring too fast, and there may not be enough time to wait for convergence to an attractor. The time-scales can also vary within the same system: as we saw in the excitable units, trajectories starting on one side of the state space converge rapidly to the attractor, whereas trajectories starting on the excitability region spend a relatively long time performing an excursion in space before reaching the attractor. This problem is made more complicated due to the fact that there are many mechanisms that can generate long - potentially arbitrarily long - transients. An example is chaotic saddles, wherein trajectories can stay indefinitely long [101]. Therefore, the behavior that is actually observed in some studies may be a transient. Moreover, some of these long-lived transients occur inside attractors. One example can be seen in ghost states

inside chaotic attractors - such as for the Logistic map or the Lorenz system - where the trajectories switch between clearly chaotic and seemingly periodic dynamics (cf. Chap. ??). Another example is the stable heteroclinic cycle: the cycle as a whole can be an attractor, but trajectories on it switch between the neighborhoods of saddle-points, describing sequences of metastable regimes. Yet another example is crawl-by motion, in which a limit cycle is in the proximity of a saddle-point. The region near the saddle-point may have very slow dynamics, and trajectories on the cycle take a long time to pass through (crawl-by) this region [102]. These examples illustrate the intricate relation between multistability - and attractors - and metastability.

Transients can play important roles. A specific example that illustrates the role of sequences of transient states is the Turing machine, the paradigmatic model for *computations* [103, 104]. It is a simple finite state machine with a head that stores a certain state and can read, write, and move along a tape. The tape is subdivided into cells containing symbols (e.g., 0's and 1's). The head represents a modern computer's central processing unit, while the tape represents the memory. Accordingly, the head follows a set of instructions that take the current state, currently read symbol on the tape and outputs the new state, the new symbol it writes on the tape, and the direction it moves. Computations are done by traversing a sequence of such state-symbol combinations. The machine may run forever - it is said to not halt -, in which case the computation is not completed. If the machine does halt, the computation is finished. From this point of view, therefore, the computation is only complete once the machine terminates the previous sequence of states. This sequence can therefore be seen as a type of transient behavior, which is crucial for the computation performed by the machine. This remark is not just an analogy - dynamical systems can be constructed that implement Turing machines [105].

More concretely, in the brain, transients have been shown to play important roles [106, 107]. There is a plethora of observations showing neural activity going through sequences of distinct states, which are all therefore transient [108, 109]. In several cases, these states are long-lived (i.e., metastable). Understanding the exact roles that *metastable regimes* play in neural circuits is crucial to understanding how they perform computations, a central question in neuroscience and also artificial intelligence [110, 111, 112]. Recent work, based on theoretical and experimental results, has shown that ghosts of saddle-node equilibria, which generate long transients, are a particularly important mechanism [110, 17, 113, 107]. It is expected, however, that other mechanisms are also present in circuits. For instance, a wide literature in neuroscience uses attractors to perform computations, and adds external perturbations to induce changes between regimes [114, 112, 109, 115]. It will be important in the future to contrast these two ideas to see the actual roles played by each of them.

To better understand the role of transients on computations in neural circuits, it is therefore important to have both an in-depth as well as a general understanding of metastable dynamics. Under this logic we developed a *general conceptual framework* for metastability, collecting and refining ideas from the neuroscience and dynamical systems literatures. As seen in Chap. ??, we proposed that the main concept behind metastability is that of long-lived transients, and showed many dynamical mechanisms capable of generating it. In the future, one can use this framework to actively compare the different mechanisms, with a view towards experiments - both biological as well as *in silico*, looking to understand how networks perform computations [110].

Besides the metastable regimes themselves, perhaps the actual *sequences* play an

important role. This is the case in the Turing machine, but there is also evidence in biological networks. An important example, already mentioned in the Introduction and in Chap. ??, showed in a series of works that sequences of metastable regimes are elicited when mice are fed tastants [116]. The sequence of regimes is unique to each tastant, suggesting they play an active role in encoding the stimuli [117]. Sequences of metastable regimes have been linked to computations in other experiments also [107, 117, 114]. In this case, a useful concept coming from dynamical systems theory is that of excitable networks by Ashwin and Postlethwaite [118, 119]. They developed methods that allow one to construct systems with prescribed connections between equilibria states. These connections may be spontaneously activated (as in connected ghosts) or via a perturbation (by perturbing across the basin boundary). This is an example of how the theory of dynamical systems is offering many tools and mechanisms that can be used to model and better understand how circuits are actually solving tasks and performing computations. This is an exciting area for future research.

Taking everything together, the field of complex systems is under intense research, with lots of us aiming to develop theory and tools to understand emergent dynamical phenomena like synchronization, the coexistence of multiple long-term solutions and the (transient) path to them. I believe that during my PhD we managed to provide some timely contributions in these directions, but there is still much to be done - with applications being very significant in biology, technology and even climate. I am very excited to help put all these pieces together.

Bibliography

- [1] Strogatz. *Nonlinear Dynamics and Chaos*. Studies in nonlinearity. Westview, 2002.
- [2] Eugene M Izhikevich. *Dynamical systems in neuroscience*. MIT press, 2007.
- [3] Anant Kant Shukla, T R Ramamohan, and S Srinivas. A new analytical approach for limit cycles and quasi-periodic solutions of nonlinear oscillators: the example of the forced Van der Pol Duffing oscillator. *Physica Scripta*, 89(7):075202, 2014.
- [4] John H. Argyris, Gunter Faust, Maria Haase, and Rudolf Friedrich. *An Exploration of Dynamical Systems and Chaos*. Springer Berlin, Heidelberg, 2 edition, 2015.
- [5] John Milnor. On the concept of attractor. *Communications in Mathematical Physics*, 99(2):177–195, 1985.
- [6] Robert L.V. Taylor. Attractors: Nonstrange to Chaotic. *SIAM Undergraduate Research Online*, 4:72–80, 2011. Publisher: Society for Industrial & Applied Mathematics (SIAM).
- [7] Henk Broer and Floris Takens. *Dynamical Systems and Chaos*. Applied Mathematical Sciences. 2011.
- [8] Jorge V. José and Eugene J. Saletan. *Classical Dynamics: A Contemporary Approach*. Cambridge University Press, Cambridge, 1998.
- [9] Paul Glendinning. *Stability, Instability And Chaos: An Introduction To The Theory Of Nonlinear Differential Equations (cambridge Texts In Applied Mathematics)*. Cambridge Texts in Applied Mathematics. Cambridge University Press, Cambridge [England], 1 edition, 1994.
- [10] Alexander N. Pisarchik and Alexander E. Hramov. Multistability in Physical and Living Systems, Characterization and Applications. *Springer Series in Synergetics*, 2022.
- [11] George Datseris and Alexandre Wagemakers. Effortless estimation of basins of attraction. *Chaos: An Interdisciplinary Journal of Nonlinear Science*, 32(2):023104, 2022.
- [12] George Datseris, Kalel Luiz Rossi, and Alexandre Wagemakers. Framework for global stability analysis of dynamical systems. *Chaos: An Interdisciplinary Journal of Nonlinear Science*, 33(7):073151, 2023.
- [13] Helena E. Nusse, James A. Yorke, and Eric J. Kostelich. Dynamics: Numerical Explorations, Accompanying Computer Program Dynamics. *Applied Mathematical Sciences*, 1994.
- [14] Maximilian Gelbrecht, Jürgen Kurths, and Frank Hellmann. Monte Carlo basin bifurcation analysis. *New Journal of Physics*, 22(3):033032, 2020.

- [15] Merten Stender and Norbert Hoffmann. bSTAB: an open-source software for computing the basin stability of multi-stable dynamical systems. *Nonlinear Dynamics*, pages 1–18, 2021.
- [16] Yuri A. Kuznetsov. Elements of Applied Bifurcation Theory. *Applied Mathematical Sciences*, 2004.
- [17] D. Koch, A. Nandan, G. Ramesan, I. Tyukin, A. Gorban, and A. Koseska. Ghost Channels and Ghost Cycles Guiding Long Transients in Dynamical Systems. *Physical Review Letters*, 133(4):047202, 2024.
- [18] Björn Sandstede. Constructing dynamical systems having homoclinic bifurcation points of codimension two. *Journal of Dynamics and Differential Equations*, 9(2):269–288, 1997.
- [19] Ed Bullmore and Olaf Sporns. Complex brain networks: graph theoretical analysis of structural and functional systems. *Nature Reviews Neuroscience*, 10(3):186–198, 2009.
- [20] Pietro Landi, Henintsoa O. Minoarivelo, Åke Brännström, Cang Hui, and Ulf Dieckmann. Complexity and stability of ecological networks: a review of the theory. *Population Ecology*, 60(4):319–345, 2018.
- [21] D J Watts and S H Strogatz. Collective dynamics of 'small-world' networks. *Nature*, 393(6684):440–442, 1998.
- [22] Stefano Boccaletti, Alexander N. Pisarchik, Charo I. del Genio, and Andreas Amann. *Synchronization: From Coupled Systems to Complex Networks*. Cambridge University Press, 2018.
- [23] Steven H. Strogatz. From Kuramoto to Crawford: exploring the onset of synchronization in populations of coupled oscillators. *Physica D: Nonlinear Phenomena*, 143(1-4):1–20, 2000.
- [24] Yoshiki Kuramoto. *Chemical Oscillations, Waves, and Turbulence*, volume 19 of *Springer Series in Synergetics*. Springer Berlin Heidelberg, Berlin, Heidelberg, 1984.
- [25] Juan A. Acebrón, L. L. Bonilla, Conrad J.Pérez Vicente, Félix Ritort, and Renato Spigler. The Kuramoto model: A simple paradigm for synchronization phenomena. *Reviews of Modern Physics*, 77(1):137–185, 2005.
- [26] Francisco A. Rodrigues, Thomas K.D.M. Peron, Peng Ji, and Jürgen Kurths. The Kuramoto model in complex networks. *Physics Reports*, 610:1–98, 2016.
- [27] Daniel A. Wiley, Steven H. Strogatz, and Michelle Girvan. The size of the sync basin. *Chaos: An Interdisciplinary Journal of Nonlinear Science*, 16(1):015103, 2006.
- [28] Yuanzhao Zhang and Steven H. Strogatz. Basins with Tentacles. *Physical Review Letters*, 127(19):194101, 2021.

- [29] Richard Taylor. There is no non-zero stable fixed point for dense networks in the homogeneous Kuramoto model. *Journal of Physics A: Mathematical and Theoretical*, 45(5):055102, 2012.
- [30] Alex Townsend, Michael Stillman, and Steven H. Strogatz. Dense networks that do not synchronize and sparse ones that do. *Chaos: An Interdisciplinary Journal of Nonlinear Science*, 30(8):083142, 2020.
- [31] Adilson E. Motter, Seth A. Myers, Marian Anghel, and Takashi Nishikawa. Spontaneous synchrony in power-grid networks. *Nature Physics*, 9(3):191–197, 2013.
- [32] Jennifer A. Dunne, Richard J. Williams, and Neo D. Martinez. Food-web structure and network theory: The role of connectance and size. *Proceedings of the National Academy of Sciences*, 99(20):12917–12922, 2002.
- [33] Patrick Crotty, Dan Schult, and Ken Segall. Josephson junction simulation of neurons. *Physical Review E*, 82(1):011914, 2010.
- [34] Micha Nixon, Moti Friedman, Eitan Ronen, Asher A. Friesem, Nir Davidson, and Ido Kanter. Synchronized Cluster Formation in Coupled Laser Networks. *Physical Review Letters*, 106(22):223901, 2011.
- [35] F Varela, J P Lachaux, E Rodriguez, and J Martinerie. The brainweb: phase synchronization and large-scale integration. *Nature Reviews Neuroscience*, 2(4):229–239, 2001.
- [36] Dirk Witthaut, Frank Hellmann, Jürgen Kurths, Stefan Kettemann, Hildegard Meyer-Ortmanns, and Marc Timme. Collective nonlinear dynamics and self-organization in decentralized power grids. *Reviews of Modern Physics*, 94(1):015005, 2022.
- [37] Pascal Fries. Rhythms for Cognition: Communication through Coherence. *Neuron*, 88(1):220–235, 2015.
- [38] W Singer. Neuronal synchrony: a versatile code for the definition of relations? *Neuron*, 24(1):49–65, 111, 1999.
- [39] Arkady Pikovsky, Michael Rosenblum, and Jürgen Kurths. *Synchronization: A Universal Concept in Nonlinear Science*, volume 70. Cambridge University Press, 2001.
- [40] Alex Arenas, Albert Díaz-Guilera, Jurgen Kurths, Yamir Moreno, and Changsong Zhou. Synchronization in complex networks. *Physics Reports*, 469(3):93–153, 2008.
- [41] R. C. Budzinski, K. L. Rossi, B. R. R. Boaretto, T. L. Prado, and S. R. Lopes. Synchronization malleability in neural networks under a distance-dependent coupling. *Physical Review Research*, 2(4):043309, 2020.
- [42] Yoshiki Kuramoto. Self-entrainment of a population of coupled non-linear oscillators. *International Symposium on Mathematical Problems in Theoretical Physics. Lecture Notes in Physics*, 39:420–422, 1975.

- [43] Adrián Ponce-Alvarez, Gustavo Deco, Patric Hagmann, Gian Luca Romani, Dante Mantini, and Maurizio Corbetta. Resting-State Temporal Synchronization Networks Emerge from Connectivity Topology and Heterogeneity. *PLOS Computational Biology*, 11(2):e1004100, 2015.
- [44] Joana Cabral, Etienne Hugues, Olaf Sporns, and Gustavo Deco. Role of local network oscillations in resting-state functional connectivity. *Neuroimage*, 57(1):130–139, 2011.
- [45] B. D. Josephson. Coupled Superconductors. *Reviews of Modern Physics*, 36(1):216–220, 1964.
- [46] Milos Marek and Ivan Stuchl. Synchronization in two interacting oscillatory systems. *Biophysical Chemistry*, 3(3):241–248, 1975.
- [47] John C. Neu. Chemical Waves and the Diffusive Coupling of Limit Cycle Oscillators. *SIAM Journal on Applied Mathematics*, 36(3):509–515, 1979.
- [48] M G Rosenblum, A S Pikovsky, and J Kurths. Phase synchronization of chaotic oscillators. *Physical Review Letters*, 76(11):1804–1807, 1996.
- [49] Réka Albert and Albert-László Barabási. Statistical mechanics of complex networks. *Reviews of Modern Physics*, 74(1):47–97, 2002.
- [50] Mark D. Humphries and Kevin Gurney. Network ‘Small-World-Ness’: A Quantitative Method for Determining Canonical Network Equivalence. *PLoS ONE*, 3(4):e2051, 2008.
- [51] Qawi K. Telesford, Karen E. Joyce, Satoru Hayasaka, Jonathan H. Burdette, and Paul J. Laurienti. The Ubiquity of Small-World Networks. *Brain Connectivity*, 1(5):367–375, 2011.
- [52] Jeffrey L. Rogers and Luc T. Wille. Phase transitions in nonlinear oscillator chains. *Physical Review E*, 54(3):R2193–R2196, 1996.
- [53] Mikail Rubinov, Rolf J F Ypma, Charles Watson, and Edward T Bullmore. Wiring cost and topological participation of the mouse brain connectome. *Proceedings of the National Academy of Sciences of the United States of America*, 112(32):10032–10037, 2015.
- [54] H. Hong, M. Y. Choi, and Beom Jun Kim. Synchronization on small-world networks. *Physical Review E*, 65(2):1–5, 2002.
- [55] Franziska Peter and Arkady Pikovsky. Transition to collective oscillations in finite Kuramoto ensembles. *Physical Review E*, 97(3):032310, 2018.
- [56] Dane Taylor, Per Sebastian Skardal, and Jie Sun. Synchronization of Heterogeneous Oscillators Under Network Modifications: Perturbation and Optimization of the Synchrony Alignment Function. *SIAM Journal on Applied Mathematics*, 76(5):1984–2008, 2016.

- [57] Lluís Arola-Fernández, Sergio Faci-Lázaro, Per Sebastian Skardal, Emanuel-Cristian Boghiu, Jesús Gómez-Gardeñes, and Alex Arenas. Emergence of explosive synchronization bombs in networks of oscillators. *Communications Physics*, 5(1):264, 2022.
- [58] R. C. Budzinski, B. R. R. Boaretto, T. L. Prado, R. L. Viana, and S. R. Lopes. Synchronous patterns and intermittency in a network induced by the rewiring of connections and coupling. *Chaos: An Interdisciplinary Journal of Nonlinear Science*, 29(12):123132, 2019.
- [59] Per Sebastian Skardal and Alex Arenas. Higher order interactions in complex networks of phase oscillators promote abrupt synchronization switching. *Communications Physics*, 3(1):218, 2020.
- [60] Hyunsuk Hong, Jaegon Um, and Hyunggyu Park. Link-disorder fluctuation effects on synchronization in random networks. *Physical Review E - Statistical, Nonlinear, and Soft Matter Physics*, 87(4):1–5, 2013.
- [61] Christopher Rackauckas and Qing Nie. DifferentialEquations.jl – A Performant and Feature-Rich Ecosystem for Solving Differential Equations in Julia. *Journal of Open Research Software*, 5(1):15, 2016.
- [62] Jeff Bezanson, Alan Edelman, Stefan Karpinski, and Viral B Shah. Julia: A fresh approach to numerical computing. *SIAM Review*, 59(1):65–98, 2017.
- [63] John D Hunter. Matplotlib: A 2D Graphics Environment. *Computing in science & engineering*, 9(3):90–95, 2007.
- [64] George Datseris, Jonas Isensee, Sebastian Pech, and Tamás Gál. DrWatson: the perfect sidekick for your scientific inquiries. *Journal of Open Source Software*, 5(54):2673, 2020.
- [65] Kalel Rossi. Repository for dynamical malleability code. *Github Repository*, 2022.
- [66] Georgi S. Medvedev. Small-world networks of Kuramoto oscillators. *Physica D: Nonlinear Phenomena*, 266:13–22, 2014.
- [67] Nicole Carlson, Dong-Hee Kim, and Adilson E. Motter. Sample-to-sample fluctuations in real-network ensembles. *Chaos: An Interdisciplinary Journal of Nonlinear Science*, 21(2):025105, 2011.
- [68] Hyunsuk Hong, Hugues Chaté, Hyunggyu Park, and Lei Han Tang. Entrainment transition in populations of random frequency oscillators. *Physical Review Letters*, 99(18):1–4, 2007.
- [69] Hyunsuk Hong, Hyunggyu Park, and Lei-Han Tang. Anomalous Binder Cumulant and Lack of Self-Averageness in Systems with Quenched Disorder. *Journal of the Korean Physical Society*, 49(5):L1885–L1889, 2006.
- [70] Steven H. Strogatz and Renato E. Mirollo. Phase-locking and critical phenomena in lattices of coupled nonlinear oscillators with random intrinsic frequencies. *Physica D: Nonlinear Phenomena*, 31(2):143–168, 1988.

- [71] Jordan G Brankov, Daniel M Danchev, and Nicholai S Tonchev. *Theory of Critical Phenomena in Finite-Size Systems*. World Scientific, 2000.
- [72] Eric J. Hildebrand, Michael A. Buice, and Carson C. Chow. Kinetic Theory of Coupled Oscillators. *Physical Review Letters*, 98(5):054101, 2007.
- [73] Paulo F. C. Tilles, Fernando F. Ferreira, and Hilda A. Cerdeira. Multistable behavior above synchronization in a locally coupled Kuramoto model. *Physical Review E*, 83(6):066206, 2011.
- [74] K. Binder. Finite size effects on phase transitions. *Ferroelectrics*, 73(1):43–67, 1987.
- [75] Per Sebastian Skardal, Dane Taylor, and Jie Sun. Optimal Synchronization of Complex Networks. *Physical Review Letters*, 113(14):144101, 2014.
- [76] Markus Brede. Synchrony-optimized networks of non-identical Kuramoto oscillators. *Physics Letters, Section A: General, Atomic and Solid State Physics*, 372(15):2618–2622, 2008.
- [77] R. Carareto, F. M. Orsatti, and J. R.C. Piqueira. Optimized network structure for full-synchronization. *Communications in Nonlinear Science and Numerical Simulation*, 14(6):2536–2541, 2009.
- [78] Lubos Buzna, Sergi Lozano, and Albert Díaz-Guilera. Synchronization in symmetric bipolar population networks. *Physical Review E*, 80(6):066120, 2009.
- [79] Didier Sornette. *Critical Phenomena in Natural Sciences, Chaos, Fractals, Self-organization and Disorder: Concepts and Tools*. Springer Series in Synergetics. 2006.
- [80] Hyunsuk Hong, Hyunggyu Park, and Lei Han Tang. Finite-size scaling of synchronized oscillation on complex networks. *Physical Review E*, 76(6):1–7, 2007.
- [81] Shai Wiseman and Eytan Domany. Lack of self-averaging in critical disordered systems. *Physical Review E*, 52(4):3469–3484, 1995.
- [82] M E Newman and D J Watts. Scaling and percolation in the small-world network model. *Physical Review E*, 60(6 Pt B):7332–7342, 1999.
- [83] Victor Buenda, Pablo Villegas, Raffaella Burioni, and Miguel A. Muoz. The broad edge of synchronization: Griffiths effects and collective phenomena in brain networks. *Philosophical Transactions of the Royal Society A*, 380(2227):20200424, 2022.
- [84] Pablo Villegas, Paolo Moretti, and Miguel A. Muñoz. Frustrated hierarchical synchronization and emergent complexity in the human connectome network. *Scientific Reports*, 4(1):5990, 2014.
- [85] G Tononi, O Sporns, and G M Edelman. A measure for brain complexity: relating functional segregation and integration in the nervous system. *Proceedings of the National Academy of Sciences*, 91(11):5033–5037, 1994.

- [86] Giulio Tononi and Gerald M. Edelman. Consciousness and Complexity. *Science*, 282(5395):1846–1851, 1998.
- [87] Gustavo Deco, Giulio Tononi, Melanie Boly, and Morten L. Kringelbach. Rethinking segregation and integration: contributions of whole-brain modelling. *Nature Reviews Neuroscience*, 16(7):430–439, 2015.
- [88] Andrew A Fingelkurts and Alexander A Fingelkurts. Timing in cognition and EEG brain dynamics: discreteness versus continuity. *Cognitive Processing*, 7(3):135–162, 2006.
- [89] Cheng-yu T. Li, Mu-ming Poo, and Yang Dan. Burst Spiking of a Single Cortical Neuron Modifies Global Brain State. *Science*, 324(5927):643–646, 2009.
- [90] Lyle Muller, Ján Mináč, and Tung T. Nguyen. Algebraic approach to the Kuramoto model. *Physical Review E*, 104(2):L022201, 2021.
- [91] Roberto C. Budzinski, Tung T. Nguyen, Jacqueline Doàn, Ján Mináč, Terrence J. Sejnowski, and Lyle E. Muller. Geometry unites synchrony, chimeras, and waves in nonlinear oscillator networks. *Chaos*, 32(3):031104, 2022.
- [92] Edward J. Hancock and Georg A. Gottwald. Model reduction for Kuramoto models with complex topologies. *Physical Review E*, 98(1):012307, 2018.
- [93] Steven Strogatz. *Sync: The Emerging Science of Spontaneous Order*. Hyperion Press, 2003.
- [94] Ulrike Feudel. Complex Dynamics In Multistable Systems. *International Journal of Bifurcation and Chaos*, 18(06):1607–1626, 2008.
- [95] Peter J. Menck, Jobst Heitzig, Norbert Marwan, and Jürgen Kurths. How basin stability complements the linear-stability paradigm. *Nature Physics*, 9(2):89–92, 2013.
- [96] Hana Krakovská, Christian Kuehn, and Iacopo P Longo. Resilience of dynamical systems. *European Journal of Applied Mathematics*, pages 1–46, 2023.
- [97] Silvan Hürkey, Nelson Niemeyer, Jan-Hendrik Schleimer, Stefanie Ryglewski, Susanne Schreiber, and Carsten Duch. Gap junctions desynchronize a neural circuit to stabilize insect flight. *Nature*, 618(7963):118–125, 2023.
- [98] K. L. Rossi, R. C. Budzinski, B. R. R. Boaretto, T. L. Prado, U. Feudel, and S. R. Lopes. Phase-locking intermittency induced by dynamical heterogeneity in networks of thermosensitive neurons. *Chaos: An Interdisciplinary Journal of Nonlinear Science*, 31(8):083121, 2021.
- [99] Everton S. Medeiros, Rene O. Medrano-T, Iberê L. Caldas, and Ulrike Feudel. Boundaries of synchronization in oscillator networks. *Physical Review E*, 98(3):030201, 2018.
- [100] George Datseris. DynamicalSystems.jl: A Julia software library for chaos and nonlinear dynamics. *Journal of Open Source Software*, 3(23):598, 2018. Publisher: The Open Journal.

- [101] Ying-Cheng Lai and Tamás Tél. *Transient Chaos: Complex Dynamics on Finite-Time Scales*. Applied Mathematical Sciences. Springer New York, NY, 2009.
- [102] Alan Hastings, Karen C. Abbott, Kim Cuddington, Tessa Francis, Gabriel Gellner, Ying-Cheng Lai, Andrew Morozov, Sergei Petrovskii, Katherine Scranton, and Mary Lou Zeeman. Transient phenomena in ecology. *Science*, 361(6406), 2018.
- [103] A. M. Turing. On Computable Numbers, with an Application to the Entscheidungsproblem. *Proceedings of the London Mathematical Society*, s2-42(1):230–265, 1937.
- [104] George S. Boolos, John P. Burgess, and Richard C. Jeffrey. *Computability and Logic*. Cambridge University Press, 5 edition, 2007.
- [105] Claire M. Postlethwaite, Peter Ashwin, and Matthew Egbert. A Continuous Time Dynamical Turing Machine. *IEEE Transactions on Neural Networks and Learning Systems*, PP(99):1–13, 2024.
- [106] Peter Ashwin and Marc Timme. When instability makes sense. *Nature*, 436(7047):36–37, 2005.
- [107] Ofer Mazor and Gilles Laurent. Transient Dynamics versus Fixed Points in Odor Representations by Locust Antennal Lobe Projection Neurons. *Neuron*, 48(4):661–673, 2005.
- [108] Emmanuelle Tognoli and J. A.Scott Kelso. The Metastable Brain. *Neuron*, 81(1):35–48, 2014.
- [109] B. A. W. Brinkman, H. Yan, A. Maffei, I. M. Park, A. Fontanini, J. Wang, and G. La Camera. Metastable dynamics of neural circuits and networks. *Applied Physics Reviews*, 9(1):011313, 2022.
- [110] Daniel Koch, Akhilesh Nandan, Gayathri Ramesan, and Aneta Koseska. Biological computations: Limitations of attractor-based formalisms and the need for transients. *Biochemical and Biophysical Research Communications*, 720:150069, 2024.
- [111] Saurabh Vyas, Matthew D. Golub, David Sussillo, and Krishna V. Shenoy. Computation Through Neural Population Dynamics. *Annual Review of Neuroscience*, 43(1):249–275, 2020.
- [112] David Sussillo and Omri Barak. Opening the Black Box: Low-Dimensional Dynamics in High-Dimensional Recurrent Neural Networks. *Neural Computation*, 25(3):626–649, 2013.
- [113] Akhilesh Nandan, Abhishek Das, Robert Lott, and Aneta Koseska. Cells use molecular working memory to navigate in changing chemoattractant fields. *eLife*, 11:e76825, 2022.
- [114] Laura N. Driscoll, Krishna Shenoy, and David Sussillo. Flexible multitask computation in recurrent networks utilizes shared dynamical motifs. *Nature Neuroscience*, 27(7):1349–1363, 2024.

- [115] Rodrigo Laje and Dean V Buonomano. Robust timing and motor patterns by taming chaos in recurrent neural networks. *Nature Neuroscience*, 16(7):925–933, 2013.
- [116] Lauren M. Jones, Alfredo Fontanini, Brian F. Sadacca, Paul Miller, and Donald B. Katz. Natural stimuli evoke dynamic sequences of states in sensory cortical ensembles. *Proceedings of the National Academy of Sciences*, 104(47):18772–18777, 2007.
- [117] Giancarlo La Camera, Alfredo Fontanini, and Luca Mazzucato. Cortical computations via metastable activity. *Current Opinion in Neurobiology*, 58:37–45, 2019.
- [118] Peter Ashwin and Claire Postlethwaite. Excitable networks for finite state computation with continuous time recurrent neural networks. *Biological Cybernetics*, 115(5):519–538, 2021.
- [119] Peter Ashwin, Muhammed Fadera, and Claire Postlethwaite. Network attractors and nonlinear dynamics of neural computation. *Current Opinion in Neurobiology*, 84:102818, 2024.

Acknowledgments

Doing a PhD is not trivial (no citation needed here, I think). It is made possible not just from one's own hard work, but with help and support from many others.

To start, the PhD was possible due to financial support from the German Academic Exchange Foundation (DAAD, in german). I am very thankful for the opportunity to do all this work with their warm support. In this sense, I am also grateful to the University of Oldenburg for the structures provided that allowed me to work.

Moving from the material to the intellectual and personal support, I am extremely grateful to Prof. Ulrike Feudel, my supervisor for all of these years! We had a lot of fun, and I learned so much from her. On top of the specific knowledge of the area, I think maybe the most important skill she developed on me was the ability to refine a thought and rigorously develop an idea until you are confident about it. On top of all the actual science we made, I find it amazing how many conferences I had the opportunity to participate in, and how many people I met - a lot of this I owe to Ulrike's support. In a similar vein I also want to deeply thank my friend and collaborator, Prof. (yes, Prof!) Everton Medeiros. Maybe without even noticing, he also taught me so much. He was a crucial aid in making this whole process a lot more fun and exciting - with, of course, better science. I will always remember this fondly - as will I remember his legendary goal from the corner of the pitch in Spiekeroog. Football's loss is academia's gain. Finally, since my Bachelor's I've always been able to count on my friends and collaborators Roberto Budzinski and Bruno Boaretto. I've counted on them for endless scientific discussions, arguments about how something should be written on a paper, and motivation. All of this always with a really nice and fun atmosphere.

Moving more to the emotional (and personal still) support, I am above all thankful to my mom and my sister for just about everything. Moving abroad is not easy - for anyone involved - but their unwavering love, warmth, and understanding made it all happen! This extends to my whole family, in fact.

Friends are also a crucial ingredient to a nice life. And in this I also have had the luck to count on some amazing figures. I will only name some - their egos will have to be satisfied. In no particular order I want to thank from the bottom of my heart Jakob and Bianca Weik, Maira Theisen, Gabriel Gubert, Lucas Polyceno, Carlos Martins, Alexandre Camargo, Rafa Jakuboski, Joao Paludo, Marcos Sato, George Datseris, Bryony Hobden, Patryk Bielski, Luis Gustavo, and Deoclecio Valente - and many others I equally love but, come on, the list was already too big.

Finally, I mentioned I met a lot of amazing people doing science, some of whom I already mentioned. For all the discussions, support, and fun, I want to especially thank Klaus Lehnertz, Lyle Muller, Pete Ashwin, Aneta Koseska, Vyacheslav Kruglov, Ryan Deeley, and Jan Freund.

Eidesstattliche Erklärung

Hiermit versichere ich, dass ich diese Dissertation selbstständig verfasst habe und nur die hier angegebenen Hilfsmittel und Quellen benutzt habe. Zudem versichere ich, dass diese Dissertation weder in ihrer Gesamtheit noch in Teilen einer anderen Hochschule zur Begutachtung in einem Promotionsverfahren vorliegt oder vorgelegen hat. Bis auf die angegebenen Teilpublikationen, ist diese Arbeit noch nicht veröffentlicht worden. Die Leitlinien guter wissenschaftlicher Praxis an der Carl von Ossietzky Universität Oldenburg wurden befolgt. Für dieses Promotionsvorhaben wurden keine kommerziellen Vermittlungs- oder Beratungsdienste in Anspruch genommen.

Oldenburg, den 07.11.2024

Kalel Luiz Rossi